

Submitted to *Journal of Geophysical Research*, April 1997

## UARS MLS $\text{HNO}_3$ observations: Implications for Antarctic PSCS

M. L. Santee,<sup>1</sup> A. Tabazadeh,<sup>2</sup> G. L. Manney,<sup>1</sup> R. J. Salawitch,<sup>1</sup> L. Froidevaux,<sup>1</sup> W. G. Read,<sup>1</sup>  
J. W. Waters<sup>1</sup>

### Abstract

We present Microwave Limb Sounder (MLS) measurements of gas-phase  $\text{HNO}_3$  obtained at the beginning of five southern hemisphere winters: 1992-1996. The observed evolution of 465 K  $\text{HNO}_3$  is compared against that predicted using nitric acid trihydrate (NAT), nitric acid dihydrate (NAD), and liquid ternary solution models of polar stratospheric cloud (PSC) composition and correlated with temperature histories from three-dimensional back trajectory calculations to infer the composition of the PSCS that formed in early winter each year. In general, we find a strong correspondence between the area of gas-phase  $\text{HNO}_3$  loss and the area of temperatures below 192 K but only a weak correspondence between the area of gas-phase  $\text{HNO}_3$  loss and the area of temperatures below 195 K, the value commonly assumed as the threshold for PSC formation. Although temperatures were low enough to maintain NAT PSCs, the MLS data clearly show that they were not forming. The MLS  $\text{HNO}_3$  observations indicate different initial compositions for the PSCS depending on the physical state of the background sulfate aerosols. If the pre-existing aerosols are liquid, then the formation of ternary solutions is initiated as the temperature drops below about 192 K, followed by a gradual conversion to NAD after exposure to low temperatures for several days.  $\text{HNO}_3$  uptake into ternary solutions occurs at higher temperatures and is more severe, and the conversion to NAD is delayed, under conditions of enhanced aerosol loading from the Mount Pinatubo eruption. The MLS measurements from 1996 show less  $\text{HNO}_3$  depletion than predicted by any of the PSC composition models. During the 1996 early southern winter the lower stratosphere was substantially colder than average, and the air masses experienced larger sustained synoptic cooling rates and spent more time at temperatures near the ice frost point than in previous years. Hence a majority of the background aerosols may have frozen, inhibiting the growth of ternary solutions but promoting formation of a metastable, water-rich,  $\text{HNO}_3$ -containing solid phase (Type Ic) characterized by a relatively high  $\text{HNO}_3$  vapor pressure, in good agreement with the MLS data.

*et al.* [1995] never observed NAT nucleation in the solution without prior formation of MixII, which then transformed into a metastable nitric acid dihydrate (NAD,  $\text{HNO}_3 \cdot 2\text{H}_2\text{O}$ ) phase within a few hours. NAT was always the last phase to form, with NAD persisting for days, in agreement with their earlier laboratory experiments on PSCs [Worsnop *et al.*, 1993] showing NAD to be only slightly less stable than NAT.

Alternatively, laboratory studies by Koop *et al.* [1995] show that ternary bulk solutions remain supercooled to temperatures below the ice frost point. They contend that only water ice is a suitable nucleation site for  $\text{H}_2\text{SO}_4$  and  $\text{HNO}_3$  hydrates, and thus stratospheric aerosol droplets must cool below the frost point before crystallization of either  $\text{HNO}_3$  or  $\text{H}_2\text{SO}_4$  in solution is possible. Meilinger *et al.* [1995] suggest that the rapid cooling rates induced by orographically forced lee waves lead to non-equilibrium conditions that facilitate freezing of the smallest ternary droplets into NAT, since their composition is the closest to that of the trihydrate. However, recent freezing experiments on  $\text{HNO}_3/\text{H}_2\text{O}$  aerosols indicate that the  $\text{HNO}_3$  concentration in solution must be larger than 1:2.5 ( $\text{HNO}_3:\text{H}_2\text{O}$ ) in order for the  $\text{HNO}_3$  to crystallize [Disselkamp *et al.*, 1996]. This result argues against the Meilinger *et al.* [1995] proposal of crystallization of aerosols containing less than a 1:3 ( $\text{HNO}_3:\text{H}_2\text{O}$ ) ratio. In addition, Tabazadeh *et al.* [1996] use aircraft observations of PSCs and a statistical analysis in which both background and lee wave temperature fluctuations are superimposed on synoptic scale temperature histories to demonstrate that neither ice crystal nucleation nor lee wave encounters are correlated with the occurrence of Type Ia PSCs. Murphy and Gary [1995] and Tabazadeh *et al.* [1996] argue that small but rapid temperature fluctuations (especially frequent in the Arctic) promote the initial formation of large numbers of small metastable particles with subsequent mass transfer to the larger, more stable NAT particles. In fact, Tabazadeh *et al.* [1996] conclude that mass transfer, and not the mesoscale cooling rate, controls the Type Ia PSC formation process; once the synoptic temperatures drop below about 192 K, the only condition necessary for Type Ia formation is that temperatures remain below the NAT frost point for longer than  $\sim 1$  day.

Building on the laboratory studies [Worsnop *et al.*, 1993; Marti and Mauersberger, 1993] indicating the initial presence of higher hydrates of  $\text{HNO}_3$ , Tabazadeh *et al.* [1995] and Tabazadeh and Toon

[1996] have postulated a third subclass of Type I PSCs, Type Ic, composed of a water-rich metastable  $\text{HNO}_3/\text{H}_2\text{O}$  solid phase that transforms into NAT or NAD over time. In their scenario, the thermal history of the air mass, and thus the physical state of the background sulfate aerosols, determines the phase of the PSCs: upon cooling, if the  $\text{H}_2\text{SO}_4$  aerosols are liquid, then Type Ib ternary solutions form; if they are frozen, then Type Ic particles initially form. Assuming that the ice frost point is not reached, if the cooling is then followed by a warming to about 196-198 K, some supercooled  $\text{H}_2\text{SO}_4/\text{H}_2\text{O}$  aerosols may freeze (as observed in the laboratory by Iraci *et al.* [1994]) and remain frozen until the air mass experiences temperatures high enough to melt SAT (about 210-220 K [Middlebrook *et al.*, 1993; Zhang *et al.*, 1993b]). With this mechanism, cooling/warming cycles eventually lead to the formation of Type Ia PSCs. This scenario is consistent with aircraft observations of PSCs in both the Arctic and the Antarctic [Tabazadeh *et al.*, 1995; Tabazadeh *et al.*, 1996], and is also supported by an analysis of balloonborne backscatter measurements of PSCs from four Arctic winters [Larsen *et al.*, 1996].

In this study we investigate PSC formation using measurements of gas-phase  $\text{HNO}_3$  made by the Microwave Limb Sounder (MLS) aboard the Upper Atmosphere Research Satellite (UARS). Although these satellite measurements lack the resolution and precision of in situ measurements, they have the important advantage of providing daily hemispheric coverage over a range of pressures and over the course of several years. Here we examine in detail the evolution of gas-phase  $\text{HNO}_3$  during the 1994 early southern winter period, and we contrast this behavior with that during similar periods in 1992, 1993, 1995 and 1996. We compare the observed  $\text{HNO}_3$  values in each year to those predicted assuming NAT, NAD, and liquid ternary solution models of PSC composition. We also use trajectory calculations to explore the correlation between temperature history and PSC composition as inferred from the MLS measurements of gas-phase  $\text{HNO}_3$ .

## 2. Measurement Description

MLS has been obtaining millimeter-wavelength thermal emission measurements in the stratosphere in both hemispheres since late September 1991. The MLS data are not degraded by the presence of PSCs or other stratospheric aerosols. The microwave limb

UARS began operating in an instrument power sharing mode whereby MLS is periodically turned off, also at that time an MLS operational schedule consisting of (typically) two days of scanning followed by one day of “rest” was adopted to conserve the lifetime of the antenna scanning mechanism. The limited data coverage and the gaps in the data for these years are evident in Figure 1, which is discussed in more detail below. Because of the short timescales involved, the sporadic data of 1992, 1995, and 1996 are not as well suited for a detailed study of PSC formation processes. In both 1993 and 1994 MLS obtained a complete set of daily limb scans during the early southern winter observing period. In this study we have chosen to examine the 1994 data more extensively for two reasons: the later onset of low temperatures and the earlier start of the observing period in 1994 (see Figure 1), capturing the initial stages of PSC formation, and the existence of data from the ASHOE campaign and the Polar Ozone and Aerosol Measurement (POAM) II instrument, providing supplementary information about environmental conditions in the polar vortex.

### 3.1. 1994 Early Southern Winter

The behavior of MLS  $\text{HNO}_3$  on selected days during the 1994 early southern winter south-viewing period (May 24 – July 3) is shown in Plate 1. The MLS data are gridded by binning and *averaging* 24 hours of data and are then vertically interpolated to the 465 K potential temperature ( $\theta$ ) surface (ranging from  $\sim 30$ –60 hPa for the low temperatures inside the polar vortex) using United Kingdom Meteorological Office (UKMO) temperatures [Swinbank and O’Neill, 1994]. Contours of temperature and potential vorticity (PV) derived from the UKMO analyses are also shown. During southern late autumn and early winter (June–July), the lower stratospheric vortex is characterized by strong diabatic descent but very little latitudinal mixing across its boundary [Manney *et al.*, 1994]. In the absence of other effects, these conditions lead to large  $\text{HNO}_3$  mixing ratios inside the vortex like those seen at the beginning of the observing period. The decreases observed in the  $\text{HNO}_3$  abundances during winter are unlikely to be caused by dynamical processes and are attributed here to PSC activity. POAM II aerosol extinction measurements confirm the existence of PSCs during this time period [Fromm *et al.*, 1997].

Although 465 K temperatures have been below 195 K over a sizeable area since mid-May (see Fig-

ure 1), gas-phase  $\text{HNO}_3$  values remain high in most regions of the vortex through the first week in June. A small pocket of low  $\text{HNO}_3$  appears in the map on June 7 and intensifies as temperatures drop below 188 K the next day (not shown). Loss of gas-phase  $\text{HNO}_3$  continues throughout the observing period, so that by the beginning of July very low  $\text{HNO}_3$  concentrations (3 ppbv or less) are measured throughout the extensive cold region.

While maps constructed from gridded data provide a visually effective means of displaying observations, they can be deceptive in that the gridding process necessarily smoothes out the contributions from individual measurements. PSCs can be highly localized phenomena, especially in early winter; given the spacing of the UARS orbit tracks, short-lived PSCs of limited geographical extent may be represented in only one or two MLS profiles, or may go undetected altogether. In Plate 2a the retrieved  $\text{HNO}_3$  mixing ratios for June 2 are shown again, this time only at the MLS measurement locations, and in Plate 2b the UKMO temperatures are shown interpolated to these locations. Relatively low  $\text{HNO}_3$  mixing ratios are recorded for a few points where the temperatures are in the range 191–193 K; although this area does register lower mixing ratios in the map of gridded data (Plate 1), the difference in mixing ratio is smaller. In this study we mostly use averaged data rather than individual measurements because of the noise associated with each retrieved profile (see Section 2). As discussed further below, the relationship between depressions in gas-phase  $\text{HNO}_3$  and variations in temperature is also explored by binning the data with respect to temperature.

The vertical extent of severely depleted gas-phase  $\text{HNO}_3$  and its relationship to low temperatures over the UARS month is illustrated in Plate 3, which shows MLS  $\text{HNO}_3$  and UKMO temperature and PV over the range 420 K to 585 K. The pink lines are contours of PV (scaled to yield similar values throughout the  $\theta$  domain) that circumscribe the boundary of the vortex; the cyan and purple lines demark the volumes within which the temperatures are below 192 K and the  $\text{HNO}_3$  mixing ratios are below 4 ppbv, respectively. The surfaces of low  $\text{HNO}_3$  along the perimeter of these plots are situated outside the vortex and are not associated with PSC formation. Temperatures in the *upper* portion of the vertical range are already low by early June, but the bottom portion of the vortex does not cool below 192 K until June 8 (although 465 K temperatures are below 195 K at this

$\text{H}_2\text{O}$  mixing ratio and total mass of sulfate present per unit volume of air. As above, a  $\text{H}_2\text{O}$  mixing ratio of 4.5 ppmv is used. We assume a total  $\text{HNO}_3$  mixing ratio of 12 ppbv based on the MLS measurements taken inside the vortex prior to significant PSC activity. This value is consistent with in situ measurements of total reactive nitrogen ( $\text{NO}_y$ ) obtained during ASHOE flights into the vortex in early June [D. Fahey, personal communication, 1996]. The mass of condensed  $\text{H}_2\text{SO}_4$  is taken to be  $0.3 \mu\text{g}/\text{m}^3$  to represent background (non-volcanic) conditions. Again, this value is consistent with vortex measurements of sulfate aerosol volume from the early June ASHOE flights [J. Wilson, personal communication, 1996]. Maps constructed from the MLS data and the ternary solution calculations are shown in Plate 5c. Comparison of Plates 5a–5c shows that NAT particles are the most efficient, and ternary droplets the least efficient, in depleting  $\text{HNO}_3$  from the gas phase. The ternary solution calculations are in much closer (albeit not perfect) agreement with the MLS data during the first days of PSC formation. Eventually, however, the ternary model underestimates the spread of  $\text{HNO}_3$  loss. For intermediate days such as June 11, the best match to the data would probably be provided by a mixture of NAD (Plate 5b) and ternary (Plate 5c) aerosols.

The relationship between the observed  $\text{HNO}_3$  and the temperature for the entire UARS month is compared to the NAT, NAD, and liquid ternary solution model curves in Plate 6. For this plot all of the 465 K MLS measurements obtained inside the polar vortex (approximately 8000 data points) were binned into 0.5 K temperature intervals and averaged (black circles, with the standard deviations represented by error bars). Despite the large amount of scatter in the MLS data, it is clear that neither the NAT (blue line) nor the NAD (green line) models match the average behavior of the MLS  $\text{HNO}_3$  over most of the temperature range. In contrast, the ternary solution model (red line) exhibits a temperature dependence similar to that of the MLS data, although it predicts too little gas-phase  $\text{HNO}_3$  loss for temperatures between 190 K and 193 K. All three models converge to match the observations obtained at the lowest temperatures, which were mainly concentrated towards the end of the month.

A comparison of the changes in the observed and predicted  $\text{HNO}_3$  values over time is presented in Plate 7. Averages of 465 K M L S  $\text{HNO}_3$  (black circles, with the standard deviations represented by er-

ror bars) are calculated from points enclosed within the annuli between the 186 K temperature contour and the 195 K, 193 K, and 191 K temperature contours. The 186 K lower limit is imposed because no allowance is made for the formation of water ice particles. Towards the end of the observing period, the 186 K lower bound eliminates most of the low- $\text{HNO}_3$  points in the vortex interior (see Plate 1) and leads to increases in the averaged mixing ratios. For each data point within these temperature contours the equilibrium vapor pressure of  $\text{HNO}_3$  over NAT, NAD and ternary solutions is calculated as described above in connection with Plate 5. Averages of the model results are also calculated within the different annuli and are depicted by blue (NAT), green (NAD), and red (ternary solution) triangles. The standard deviations in the model averages are indicated by the cross-hatched areas.

The assumption of a NAT composition for PSCs leads to very low  $\text{HNO}_3$  vapor concentrations that are inconsistent with the MLS observations from late May and early June. The NAD model predicts  $\text{HNO}_3$  values that match the data closely during the latter half of the observing period; although the initial trend for NAD is similar to that seen in the data for the 195 K contour average, agreement with the data is much poorer for the averages at lower temperatures. In contrast, the behavior predicted for a ternary solution composition is in good agreement with the data during the early stages of  $\text{HNO}_3$  depletion for all three temperature contour averages, with the best agreement attained at the lowest temperatures. Comparison of Plate 7 and Figure 2 shows that significant incorporation of  $\text{HNO}_3$  into the ternary solution aerosols does not occur until the average temperatures drop below  $\sim 192$  K.

The sensitivity of the model calculations to the assumed water vapor mixing ratio and sulfate aerosol loading and the temperature is illustrated in Plate 8. For all cases shown the averages are calculated from points enclosed within the annulus between the 186 K and 195 K temperature contours using a total  $\text{HNO}_3$  mixing ratio of 12 ppbv; these results can be compared to those of the top panel of Plate 7. (In general the model calculations exhibit much less sensitivity for averages computed within the 191 K temperature contour). In Plate 8a the water vapor mixing ratio is varied between the extremes of 3 and 6 ppmv (using the nominal UKMO temperatures and background aerosol conditions). Although the MLS data indicate water vapor mixing ratios on the order of

### 3.2. 1992 Early Southern Winter

At the start of the 1992 early southern winter south-viewing period on June 2 (Plate 9),  $\text{HNO}_3$  abundances are high (due to diabatic descent, as discussed above) in the portion of the vortex where temperatures are above  $\sim 195$  K. However, a deficit in gas-phase  $\text{HNO}_3$  is apparent inside most (but not all) of the region where temperatures are below  $\sim 195$  K, more or less conforming to the pattern expected for crystalline Type I PSCs. These observations are in contrast to the large  $\text{HNO}_3$  mixing ratios observed throughout most of the vortex, including the low-temperature region, in early June 1994 (see Plate 1 and Figure 1). Operational constraints precluded the acquisition of additional data during 1992 until June 15 (Plate 9), by which time temperatures over a broad region have dropped below 188 K and  $\text{HNO}_3$  maps for the two years appear substantially similar.

The difference in the behavior of MLS  $\text{HNO}_3$  during early June in 1992 as compared to 1994 is probably related to the sulfate aerosol loading following the eruption of Mount Pinatubo [e.g., Tabazadeh *et al.*, 1994b; Carslaw *et al.*, 1994]. Russell *et al.* [1996] have shown that the stratospheric particle optical depth in April 1992 at 60°–700°S was enhanced by roughly a factor of 20–30 over pre-Pinatubo levels. In Plate 10 we show  $\text{HNO}_3$  maps constructed for June 2 from the MLS data and the various PSC composition models using a  $\text{H}_2\text{O}$  mixing ratio of 4.5 ppmv and a total  $\text{HNO}_3$  mixing ratio of 12 ppbv, as discussed in connection with Plate 5, and a total sulfate mass of  $10 \mu\text{g}/\text{m}^3$  to represent the Pinatubo enhancement. Although the ternary model significantly underestimates the  $\text{HNO}_3$  uptake for sulfate mass loadings of  $0.3 \mu\text{g}/\text{m}^3$  and  $3 \mu\text{g}/\text{m}^3$  (not shown), it agrees fairly well with the data for a sulfate mass of  $10 \mu\text{g}/\text{m}^3$ . However, the models constrained by the thermodynamics of NAD and NAT also agree reasonably well with the observed  $\text{HNO}_3$ . The single MLS observation day at the beginning of the 1992 early southern winter does not allow us to definitively distinguish between any of the compositions. However, the temperature dependence of the  $\text{HNO}_3$  measurements obtained inside the polar vortex during the course of the observing period, shown in Plate 11, appears to confirm that a ternary solution model using a sulfate mass of  $10 \mu\text{g}/\text{m}^3$  provides a good fit to the MLS data.

### 3.3. 1993 Early Southern Winter

As in 1994, MLS obtained a complete set of daily limb scans during the 1993 early southern winter south-looking period (May 29 – July 7; selected days shown in Plate 12). Unlike in 1994, however, in 1993 MLS did not resume south-viewing in time to capture the incipient stage of PSC formation. As indicated in Figure 1, the areal extent of  $\text{HNO}_3$  mixing ratios below 4 ppbv measured on the first day of the 1993 observing period is not achieved in 1994 until  $\sim$ June 9, midway through that observing period. The relationship between low  $\text{HNO}_3$  and low temperature for these days is different in the two years: in 1993, the areal extent of low  $\text{HNO}_3$  values is comparable to that of temperatures below 192 K, but in 1994 it is much smaller. In fact, in 1994 the areal extent of low  $\text{HNO}_3$  remains smaller than that of temperatures below 190 K for several days. A possible explanation for this difference is the lingering aftereffects in 1993 of the eruption of Mount Pinatubo. Russell *et al.* [1996] have shown that the stratospheric particle optical depth in April 1993 at 60°–700°S was still enhanced by roughly a factor of 10 over pre-Pinatubo levels. Equilibrium calculations have demonstrated that  $\text{HNO}_3$  uptake into ternary solutions occurs at higher temperatures and is more severe under volcanic conditions [Carslaw *et al.*, 1994; Tabazadeh *et al.*, 1994 b].

The  $\text{HNO}_3$ /temperature relationship inside the vortex for this observing period (Plate 13) shows that a ternary solution model using a total sulfate mass of  $3 \mu\text{g}/\text{m}^3$  to account for the residual Pinatubo enhancement produces a good fit to the MLS data. In Plate 14 the changes over time in the observed  $\text{HNO}_3$  mixing ratios are compared to those predicted by the various PSC composition models (using a  $\text{H}_2\text{O}$  mixing ratio of 4.5 ppmv, a total  $\text{HNO}_3$  mixing ratio of 12 ppbv, and a total sulfate mass of  $3 \mu\text{g}/\text{m}^3$ ). As was seen for the 1994 data, the NAT model severely underestimates the observed  $\text{HNO}_3$  abundances, while the NAD model predictions match the data closely in the latter half of the observing period and the ternary model provides excellent agreement initially.

Comparison of Plate 14 with Plate 7 reveals that the ternary calculations provide a good fit to the data after PSC formation begins for a much longer duration in 1993 than in 1994. This is probably related to the significant differences in composition between ternary solutions formed under volcanic conditions and those formed under background aerosol conditions [Tabazadeh *et al.*, 1994b]. These compositional

*et al.*, 1989]. Thus it seems unlikely that the  $\text{H}_2\text{O}$  mixing ratios could have dropped to relatively low levels while the  $\text{HNO}_3$  mixing ratios remained undiminished.

Alternatively, it maybe that temperatures fell to sufficiently low values sufficiently quickly that a majority of the background sulfate aerosols froze, precluding the formation of ternary solutions. The presence of at least some frozen sulfate cores would promote the growth of a  $\text{HNO}_3/\text{H}_2\text{O}$  solid phase referred to as a Type Ic PSC by *Tabazadeh and Toon [1996]*. Laboratory studies of the deposition of  $\text{H}_2\text{O}$  and  $\text{HNO}_3$  vapors onto a solid surface (either glass or SAT) [*Hanson, 1992; Marti and Mauersberger, 1993; Iraciet et al., 1995*] have found evidence for the formation of a **metastable** water-rich  $\text{HNO}_3$ -containing solid phase over which the  $\text{HNO}_3$  vapor pressure is relatively high (as much as 10–20 times higher than that over NAT). As this  $\text{HNO}_3/\text{H}_2\text{O}$  solid phase would also be characterized by a higher  $\text{HNO}_3$  vapor pressure than a ternary solution, its formation could explain the initial discrepancy between the ternary model and the MLS data in Plate 18a. In this case, the better agreement between the measured  $\text{HNO}_3$  and the NAD model at the end of the observing period could indicate the transfer of vapor from the water-rich solid to NAD as the particles age. Evidence to **support the formation of a water-rich  $\text{HNO}_3/\text{H}_2\text{O}$  solid phase has also been reported by *Tabazadeh et al. [1995]* and *Tabazadeh and Toon [1996]*** from an analysis of aircraft observations of PSCs in both the Arctic and the Antarctic. They found the initial depletion of gas-phase  $\text{HNO}_3$  due to a Type Ic PSC to be only about 2-3 ppbv, which corresponds very closely to the MLS observations shown in Plate 18.

#### 4. Trajectory Calculations

In the PSC formation scenario of *Tabazadeh et al. [1994a; 1995; 1996]* briefly described above, the thermal history of the air mass is critical to the phase of the PSC since it determines the physical state of the pre-existing aerosols. These aerosols are liquid in an air mass that either has never been exposed to temperatures low enough for the  $\text{H}_2\text{SO}_4$  to freeze as SAT (i.e., near the ice frost point [e.g., *Middlebrook et al., 1993; Koop et al., 1995*]) or **has recently experienced temperatures high enough for SAT to melt** (i.e., about 210–220 K [*Middlebrook et al., 1993; Zhang et al., 1993b*]). On the other hand, the aerosols may **freeze through a cooling to temperatures mar the ice**

frost point. In addition, *Tabazadeh et al. [1995]* have proposed that, after experiencing low temperatures, the  $\text{H}_2\text{SO}_4$  aerosols may crystallize to SAT upon subsequent warming to about 196–198 K (as observed in the laboratory by *Iraciet et al. [1994]*).

To investigate the correlation between synoptic-scale temperature history and PSC composition as inferred from MLS measurements of gas-phase  $\text{HNO}_3$ , we perform 20-day back trajectory calculations for selected days in each year. As described in more detail by *Manney et al. [1994]*, the three-dimensional calculations use horizontal winds and temperatures from the UKMO data assimilation system [*Swinbank and O'Neill, 1994*]. The trajectory code is formulated in isentropic coordinates and employs a standard fourth-order Runge-Kutta scheme. To account for diabatic effects, a recent version of the middle atmosphere radiation code (MIDRAD) first described by *Shine [1987]* is used to compute vertical velocities ( $d\theta/dt$ ). Since MLS data do not provide uninterrupted daily coverage, a climatological ozone field is used for the radiation calculations. The impact on the heating rates of using climatological rather than MLS ozone was determined to be negligible by *Manney et al. [1994]*. Although in general the large scale air motion is simulated well by these calculations, *Manney et al. [1995]* found that they underestimated the magnitude of the diabatic descent in the 1992 Antarctic early winter, based on comparisons with passive tracers measured by CLAES on UARS.

For each trajectory run parcels are initialized at 465 K in a box defined within the region inside the vortex where  $\text{HNO}_3$  mixing ratios are below 4 ppbv; the total number of parcels in the box is chosen to be 100 (10 on a side), 400 (20 on a side) or 900 (30 on a side) depending on the geographic extent of the  $\text{HNO}_3$  depletion on that day. The initialization time is 12UT and parcel positions are saved every four hours. Temperature histories are then constructed by interpolating UK MO temperatures (available once daily, at 12 UT) to the time, latitude, longitude, and  $\theta$  values of these parcels throughout the 20-day run. Overall diabatic effects are found to be essentially similar for runs in all five years, with parcels descending approximately 20 K in the 20 days leading up to the initialization day.

Temperature histories for selected days during the 1994 [°SC formation period are shown in Figure 4. Parcels initialized inside the small area of depleted  $\text{HNO}_3$  on June 7 (see Plate 1) had experienced a fairly flat synoptic temperature trend (Figure 4a) prior to

occasions, after which some portion of the parcels encountered temperatures above 196 K. By May 25 and 26 (Figures 7b,c), the parcels had been exposed to temperatures below 192 K for more than 6 days and below 188 K for 2 days, and by May 28 (Figure 7d) the parcels had been exposed to temperatures below 192 K for 11 days and below 188 K for 5 days, yet in all these cases the MLS data indicate higher gas-phase  $\text{HNO}_3$  values than predicted by any of the PSC composition models (see Plate 18). The parcels originating within the low- $\text{HNO}_3$  region on these days experienced larger sustained synoptic cooling rates and spent more time at temperatures near the ice frost point than in previous years. Hence a larger fraction of the sulfate aerosols may have frozen in the early winter of 1996, inhibiting the growth of ternary solutions. The presence of frozen sulfate cores would lead to the emergence of Type Ic PSCs, whose relatively high  $\text{HNO}_3$  vapor pressure provides the best match to the pattern of depletion seen in the 1996 MLS  $\text{HNO}_3$  data.

The majority of the MLS  $\text{HNO}_3$  measurements obtained during the early southern winter periods indicate that exposure to low temperatures for at least several days (longer under conditions of enhanced aerosol loading following volcanic eruptions) is necessary for a significant degree of crystalline PSC formation. This suggests the existence of substantial free-energy barriers to nucleation for the crystalline forms. Large barriers to nucleation would result in activation and growth of only a small fraction of available condensation nuclei (regardless of the cooling rates) and thus would lead to formation of a small number of relatively large  $\text{HNO}_3$ -containing particles that could fall appreciable distances, consistent with the scenario for denitrification first proposed by Salawitch *et al.* [1989].

## 5. Summary

We have examined MLS  $\text{HNO}_3$  measurements obtained at the beginning of five southern hemisphere winters: 1992–1996. The observed evolution of the gas-phase  $\text{HNO}_3$  was compared against that predicted by NAT [Hanson and Mauersberger, 1988], NAD [Worsnop *et al.*, 1993], and liquid ternary solution [Tabazadeh *et al.*, 1994b] models and correlated with temperature histories from three-dimensional back trajectory calculations to infer the composition of the PSCs that formed in early winter each year.

[In general, we have found a strong correspondence

between the area of gas-phase  $\text{HNO}_3$  loss and the area of temperatures below 192 K but only a weak correspondence between the area of gas-phase  $\text{HNO}_3$  loss and the area of temperatures below 195 K, the value commonly assumed as the threshold for PSC formation. In fact, for the three years in which MLS made measurements at or near the time of initial PSC formation (1993, 1994, and 1996), large NAT supersaturations persisted for days to weeks before significant depletion of gas-phase  $\text{HNO}_3$  occurred. Although the temperatures were low enough to maintain NAT PSCs, the MLS data clearly indicate that they were not forming. While good agreement is found at different stages of the PSC formation process between the MLS data and the ternary solution and NAD models, at no time do the MLS data match a NAT composition. This is supportive of the suggestion of a lower barrier to nucleation for NAD than for NAT [Worsnop *et al.*, 1993; Düsselkamp *et al.*, 1996].

The MLS  $\text{HNO}_3$  observations indicate that the first PSCs to form are composed of either liquid ternary solutions or a metastable water-rich solid phase, depending on the physical state of the background sulfate aerosols. This is consistent with the PSC formation scenario of Tabazadeh *et al.* [1994a; 1995; 1996]. According to this scenario, if the pre-existing aerosols are liquid, then ternary solutions form as the temperature drops below about 192 K, a few degrees below the NAT condensation point. After prolonged exposure to low temperatures, NAT or NAD particles begin to nucleate and a mixed cloud results while a transfer of  $\text{HNO}_3$  vapor from the ternary solution droplets to the more stable crystalline particles takes place, with eventual complete conversion. This paradigm can explain the MLS 1994 observations, which show better agreement with the ternary solution model in the initial stages of PSC formation but which are fit best by the NAD model as time progresses and the air masses have been exposed to low temperatures for several days. Although the 1995 MLS data are too sparse to allow a definitive conclusion, they also appear to be consistent with this PSC formation scenario.

The basic PSC formation process outlined above also applies to MLS measurements from 1993, when the stratospheric particle optical depth was still elevated by roughly a factor of 10 from the eruption of Mount Pinatubo [Russell *et al.*, 1996]. However, the 1993 MLS data indicate that  $\text{HNO}_3$  uptake into ternary solutions occurs at higher temperatures and is more severe under enhanced aerosol conditions, as predicted by Carslaw *et al.* [1994] and Tabazadeh

- spheric cloud in the Antarctic, *J. Geophys. Res.*, *94*, 11,299-11,315, 1989.
- FOX, L. E., D. R. Worsnop, M. S. Zahniser, and S. C. Wofsy, Metastable phases in polar stratospheric aerosols, *Science*, *267*, 351-355, 1995.
- Fromm, M. D., et al., Observations of Antarctic polar stratospheric clouds by POAM II in 1994 and 1995, *J. Geophys. Res.*, in press, 1997.
- Hanson, D., The uptake of  $\text{HNO}_3$  onto ice, NAT, and frozen sulfuric acid, *Geophys. Res. Lett.*, *19*, 2063-2066, 1992.
- Hanson, D. and K. Mauersberger, Laboratory studies of the nitric acid trihydrate: Implications for the south polar stratosphere, *Geophys. Res. Lett.*, *15*, 855-858, 1988.
- Iraci, L. T., A. M. Middlebrook, M. A. Wilson, and M. A. Tolbert, Growth of nitric acid hydrates on thin sulfuric acid films, *Geophys. Res. Lett.*, *21*, 867-870, 1994.
- Iraci, L. T., A. M. Middlebrook, and M. A. Tolbert, Laboratory studies of the formation of polar stratospheric clouds: Nitric acid condensation on thin sulfuric acid films, *J. Geophys. Res.*, *100*, 20,969-20,977, 1995.
- Kawa, S. R., et al., The Arctic polar stratospheric cloud aerosol: Aircraft measurements of reactive nitrogen, total water, and particles, *J. Geophys. Res.*, *97*, 7925-7938, 1992.
- Kelly, K. K., et al., Dehydration in the lower Antarctic stratosphere during late winter and early spring, 1987, *J. Geophys. Res.*, *94*, 11,317-11,357, 1989.
- Koop, T., et al., Do stratospheric aerosol droplets freeze above the ice frost point?, *Geophys. Res. Lett.*, *22*, 917-920, 1995.
- Kumer, J. B. et al., Comparison of correlative data with  $\text{HNO}_3$  version 7 from the CLAES instrument deployed on the NASA Upper Atmosphere Research Satellite, *J. Geophys. Res.*, *101*, 9621-9656, 1996.
- Larsen, N., B. M. Knudsen, J. M. Rosen, N. T. Kjome, and E. K. Yro, Balloonborne backseat ter observations of type 1 PSC formation: Inference about physical state from trajectory analysis, *Geophys. Res. Lett.*, *23*, 1091-1094, 1996.
- Manney, G. L., R. W. Zurek, A. O'Neill, and R. Swinbank, On the motion of air through the stratospheric polar vortex, *J. Atmos. Sci.*, *51*, 2973-2994, 1994.
- Manney, G. L. et al., Lagrangian transport calculations using UARS data. Part I: Passive tracers, *J. Atmos. Sci.*, *52*, 3049-3068, 1995.
- Manney, G. L., R. Swinbank, S. P. Massie, M. E. Gelman, A. J. Miller, R. Nagatani, A. O'Neill, and R. W. Zurek, Comparison of U. K. Meteorological Office and U. S. National Meteorological Center stratospheric analyses during northern and southern winter, *J. Geophys. Res.*, *101*, 10,311-10,334, 1996.
- Marti, J. and K. Mauersberger, Laboratory simulations of PSC particle formation, *Geophys. Res. Lett.*, *20*, 359-362, 1993.
- McCormick, M. P., H. M. Steele, P. Hamill, W. P. Chu, and T. J. Swisler, Polar stratospheric cloud sightings by SAM II, *J. Atmos. Sci.*, *39*, 1387-1397, 1982.
- Meilinger, S. K., T. Koop, B. P. Luo, T. Huthwelker, K. S. Carslaw, U. Krieger, P. J. Crutzen, and T. Peter, Size-dependent stratospheric droplet composition in lee wave temperature fluctuations and their potential role in PSC freezing, *Geophys. Res. Lett.*, *22*, 3031-3034, 1995.
- Middlebrook, A. M., et al., Fourier transform-infrared studies of thin  $\text{H}_2\text{SO}_4/\text{H}_2\text{O}$  films: Formation, water uptake, and solid-liquid phase changes, *J. Geophys. Res.*, *98*, 20,473-20,481, 1993.
- Molina, M. J., et al., Physical chemistry of the  $\text{H}_2\text{SO}_4/\text{HNO}_3/\text{H}_2\text{O}$  system: Implications for polar stratospheric clouds, *Science*, *216*, 1418-1423, 1993.
- Murphy, D. M. and B. L. Gary, Mesoscale temperature fluctuations and polar stratospheric clouds, *J. Atmos. Sci.*, *52*, 1753-1760, 1995.
- Pueschel, R. F., et al., Condensed nitrate, sulfate, and chloride in Antarctic stratospheric aerosols, *J. Geophys. Res.*, *94*, 11,271-11,284, 1989.
- Ravishankara, A. R. and D. R. Hanson, Differences in the reactivity of Type I polar stratospheric clouds depending on their phase, *J. Geophys. Res.*, *101*, 3885-3890, 1996.
- Russell, P. B., et al., Global to microscale evolution of the Pinatubo volcanic aerosol derived from diverse measurements and analyses, *J. Geophys. Res.*, *101*, 18,745-18,763, 1996.
- Salawitch, R. J., G. P. Gobbi, S. C. Wofsy, and M. B. McElroy, Denitrification in the Antarctic stratosphere, *Nature*, *339*, 525-527, 1989.
- Santee, M. L., et al., Interhemispheric differences in polar stratospheric  $\text{HNO}_3$ ,  $\text{H}_2\text{O}$ ,  $\text{ClO}$ , and  $\text{O}_3$ , *Science*, *267*, 849-852, 1995.
- Santee, M. L., G. L. Manney, W. G. Read, L. Froidevaux, and J. W. Waters, Polar vortex conditions during the 1995-96 Arctic winter: MLS  $\text{ClO}$  and  $\text{HNO}_3$ , *Geophys. Res. Lett.*, *23*, 3207-3210, 1996.
- Shine, K. P., The middle atmosphere in the absence of dynamic heat fluxes, *Q. J. R. Meteorol. Soc.*, *113*, 603-633, 1987.
- Solomon, S., Progress towards a quantitative understanding of Antarctic ozone depletion, *Nature*, *347*, 347-354, 1990.

**Figure 1.** The area poleward of 60°S on the 465 K potential temperature surface (expressed as the percent of the hemisphere) as a function of time within which Microwave Limb Sounder (MLS)  $\text{HNO}_3$  mixing ratios are below 4 ppbv (filled triangles) and United Kingdom Meteorological Office (UK MO) temperatures are below 188 K (dash-dot lines), 190 K (solid lines), 192 K (dotted lines) and 195 K (dashed lines). Data for all five southern hemisphere early-winter south-looking periods are shown. The filled triangles denote the days on which MLS performed full vertical scans in each year; data gaps in 1992, 1995 and 1996 are evident (see text),

Plate 1. Maps of MLS  $\text{HNO}_3$  (ppbv) for selected days during the 1994 early southern winter south-viewing period, interpolated onto the 465 K potential temperature surface using UKMO temperatures. The maps are polar orthographic projections extending to the equator, with the Greenwich meridian at the top and dashed black circles at 30° S and 60°S; blank spaces represent data gaps or bad data points. Superimposed in white are two contours of UKMO PV:  $-0.25 \times 10^4 \text{Km}^2\text{kg}^{-1}\text{s}^{-1}$  (to represent the approximate edge of the winter polar vortex at this level) and  $-0.30 \times 10^4 \text{Km}^2\text{kg}^{-1}\text{s}^{-1}$  (a second contour to indicate the steepness of the PV gradient and thus the strength of the vortex). Superimposed in black are two contours of UKMO temperature: 195 K (the approximate existence threshold for Type I PSCs) and 188 K (the ice frost point).

Plate 2. (a) 465 K  $\text{HNO}_3$  mixing ratios shown at the MLS measurement locations, with no horizontal binning or averaging performed, for June 2, 1994. (b) 465 K UKMO temperatures for June 2, 1994, interpolated to the latitude/longitude coordinates of the MLS measurements.

Plate 3. Plots illustrating the three-dimensional relationship between low temperature and severely-reduced gas-phase  $\text{HNO}_3$  inside the polar vortex for selected days during the 1994 early southern winter south-viewing period. The vertical coordinate is potential temperature, ranging from 420 K to 585 K. Latitude circles are shown at 60°S and 80°S and longitudes 0° and 90°E are labelled. The pink surface shows the  $1.4 \text{ s}^{-1}$  contour of scaled PV (corresponding to the  $-0.30 \times 10^4 \text{Km}^2\text{kg}^{-1}\text{s}^{-1}$  PV contour at 465 K, see *Manney et al.* [1994]), which represents the approximate boundary of the polar vortex. The cyan surface shows the 192 K contour of UKMO temperature. The purple surface shows the 4 ppbv contour of MLS  $\text{HNO}_3$ . The surfaces of low  $\text{HNO}_3$  along the perimeter of these plots are situated outside the vortex and are not associated with PSC formation; the geographic coverage of the  $\text{HNO}_3$  plot is terminated at 60° S to minimize the presence of these surfaces. Different perspectives are used on each day to obtain the most unobstructed view of the vortex.

Plate 4. Time series of 465 K MLS  $\text{HNO}_3$  (a) and UKMO temperatures (b) as a function of PV for the 1994 early southern winter south-viewing period. PV is expressed in terms of equivalent latitude (see text). PV contours representing the approximate edge of the winter polar vortex (see Plate 1) are overlaid in black.

Plate 5a. 465 K maps constructed from both MLS  $\text{HNO}_3$  measurements and model calculations of the equilibrium vapor pressure of  $\text{HNO}_3$  over nitric acid trihydrate (NAT), using the formula of *Hanson and Mauersberger [1988]* and a  $\text{H}_2\text{O}$  mixing ratio of 4.5 ppmv, for the days during the 1994 early southern winter south-viewing period shown in Plate 1. The maps are constructed using the model values for  $\text{HNO}_3$  inside the region where the temperature is between 186 K and 196 K and the MLS measurements of  $\text{HNO}_3$  outside of this region; this provides a picture of what MLS would have observed if NAT had been forming according to the thermodynamic expression of *Hanson and Mauersberger [1988]*,

Plate 5b. As in Plate 5a, for nitric acid dihydrate (NAD) using the thermodynamic expression of *Worsnop et al. [1993]*.

Figure 3. As in **Figure 2**, for the 1996 early southern winter south-viewing period. Again, the minimum temperatures within the vortex as a whole, which are not shown, are much lower.

**Figure 4.** Temperature histories along 20-day back trajectories for the ensemble of parcels located within the region inside the vortex where  $\text{HNO}_3$  concentrations are less than 4 ppbv on (a) **June 7, 1994**, (b) **June 11, 1994**, (c) **June 13, 1994**, and (d) **June 16, 1994**. Dashed lines indicate  $T = 188$  K and 192 K. The black circles represent the average temperatures of these parcels at each time step (every four hours) and the error bars represent the standard deviations in the averages.

**Figure 5.** As in Figure 4, for (a) May 29, 1993, (b) June 1, 1993, (c) June 2, 1993, and (d) June 7, 1993.

**Figure 6.** As in Figure 4, for (a) June 2, 1992 and (b) June 7, 1995.

**Figure 7.** As in Figure 4, for (a) May 22, 1996, (b) May 25, 1996, (c) May 26, 1996, and (d) May 28, 1996.

**Plate 12.** As in Plate 1, for the 1993 early southern winter south-viewing period.

**Plate 13.** As in Plate 6, for the 1993 early southern winter south-viewing period. The averages represent approximately 8500 MLS data points inside the polar vortex. The ternary model curve was calculated using a sulfate mass loading of  $3 \mu\text{g}/\text{m}^3$  to account for the residual **Pinatubo** enhancement.

**Plate 14.** As in Plate 7, for the 1993 early southern winter south-viewing period, using a total  $\text{HNO}_3$  mixing ratio of 12 ppbv, a  $\text{H}_2\text{O}$  mixing ratio of 4.5 ppmv, and a total sulfate mass of  $3 \mu\text{g}/\text{m}^3$ .

**Plate 15.** As in Plate 1, for the 1995 early southern winter south-viewing period.

**Plate 16.** As in Plate 1, for the 1996 early southern winter south-viewing period.

**Plate 17.** As in Plate 6, for the 1996 early southern winter south-viewing period. The averages represent approximately 2800 MLS data points inside the **polar vortex**.

**Plate 18a.** As in Plate 7, for the 1996 early southern winter south-viewing period, using a  $\text{HNO}_3$  mixing ratio of 12 ppbv, **background aerosol conditions**, and a  $\text{H}_2\text{O}$  mixing ratio of 4.5 ppmv.

**Plate 18b.** As in Plate 18a, for a  $\text{H}_2\text{O}$  mixing ratio of 3.0 ppmv.

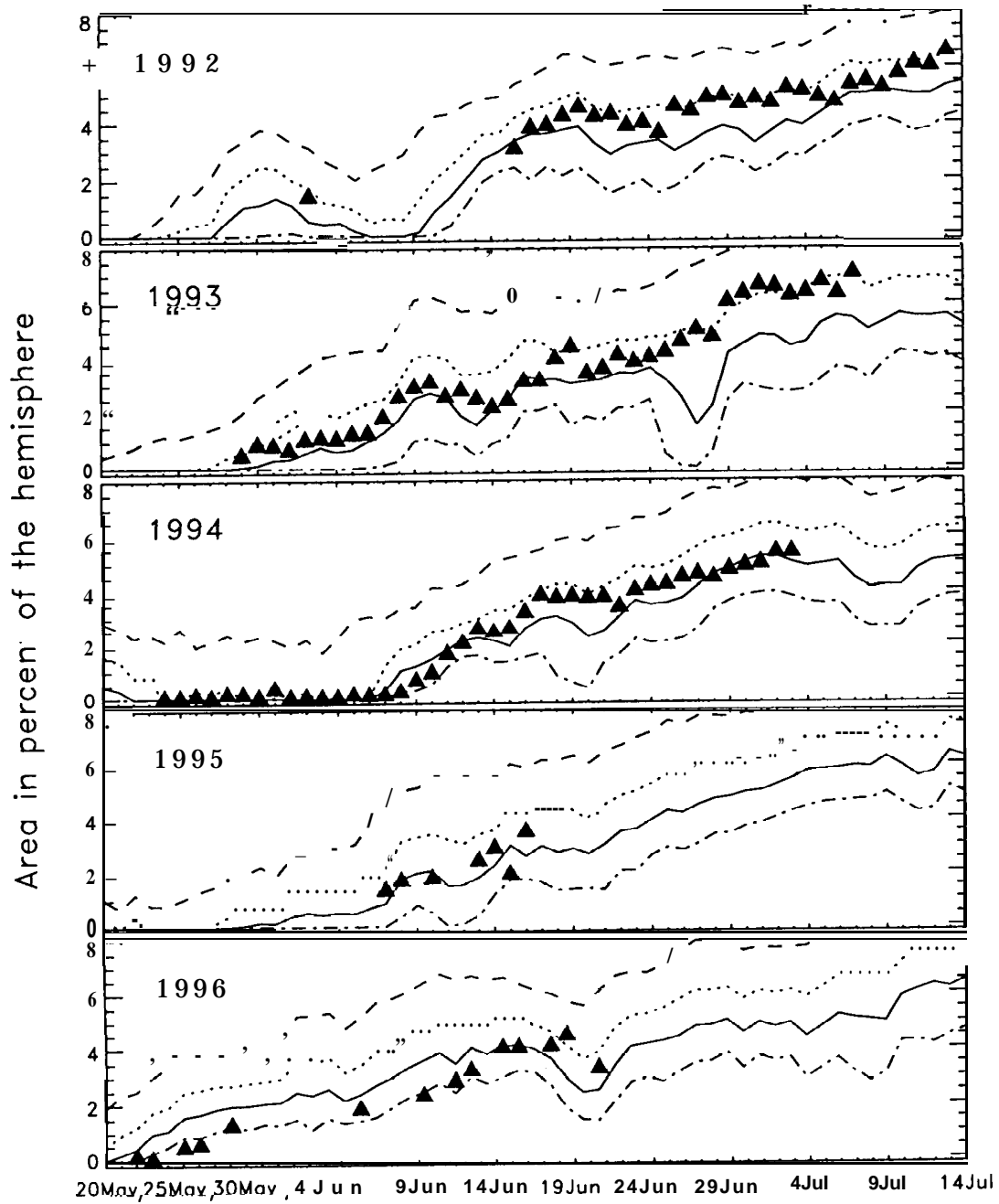
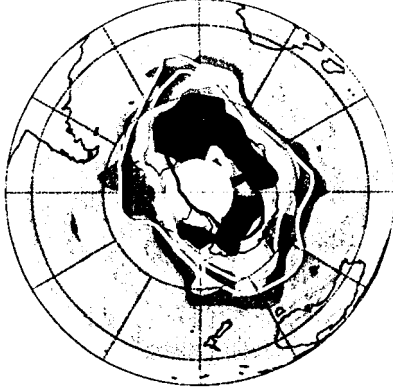


Figure 1

1994

June 2



June 7



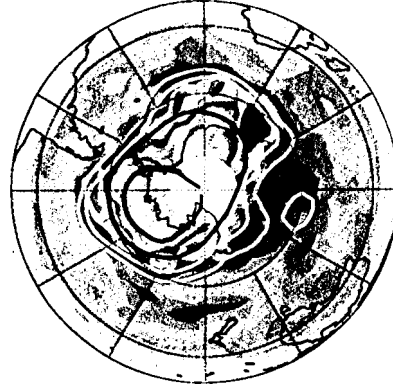
June 11



June 13



June 16



July 2

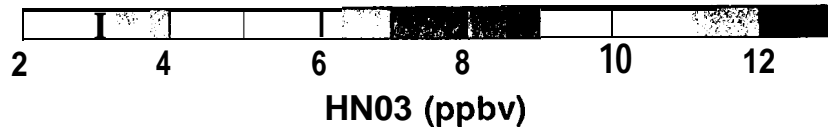
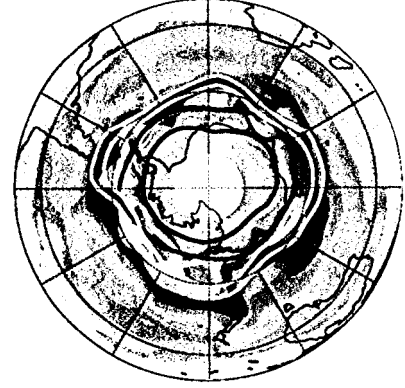
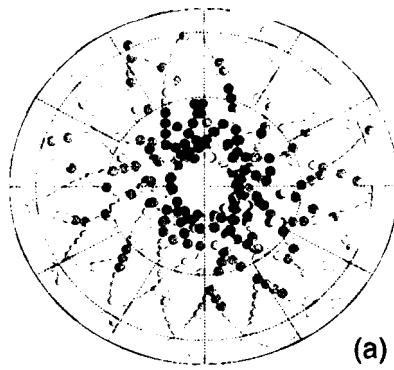


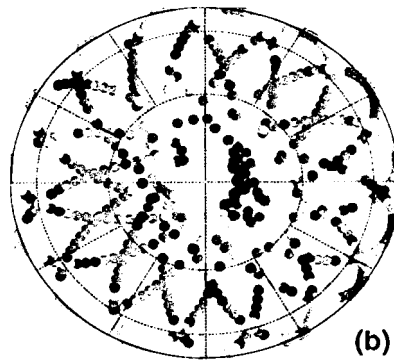
Plate 1



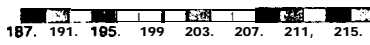
(a)



HN03 (ppbv)



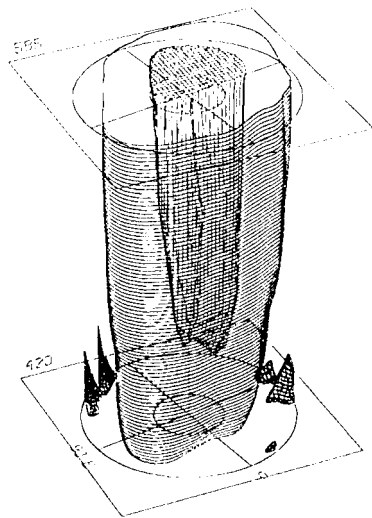
(b)



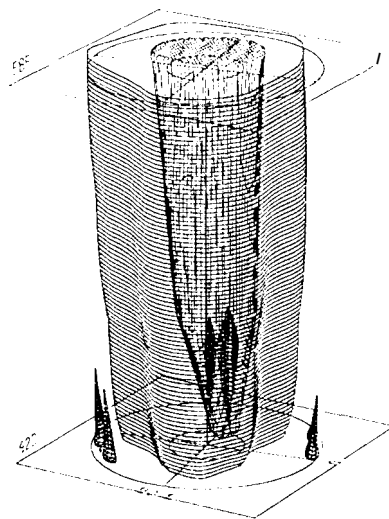
T (K)

1994

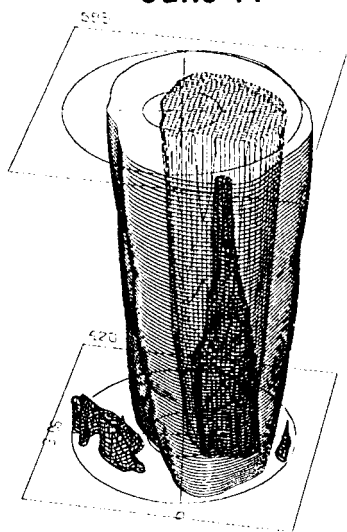
June 7



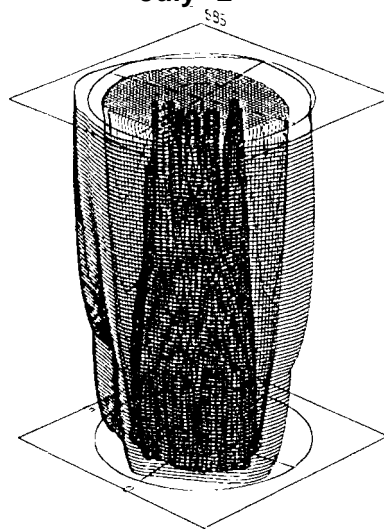
June 8



June 11



July 2



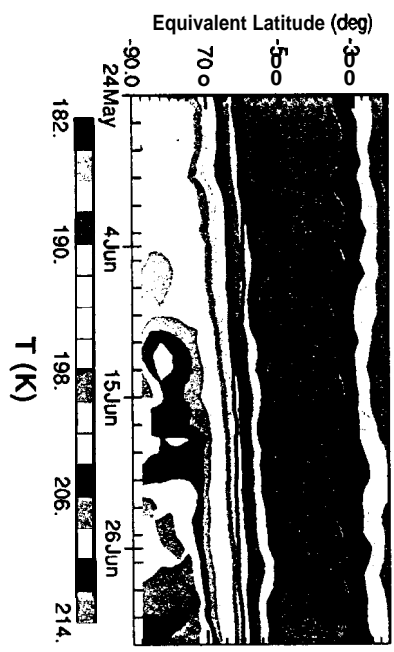
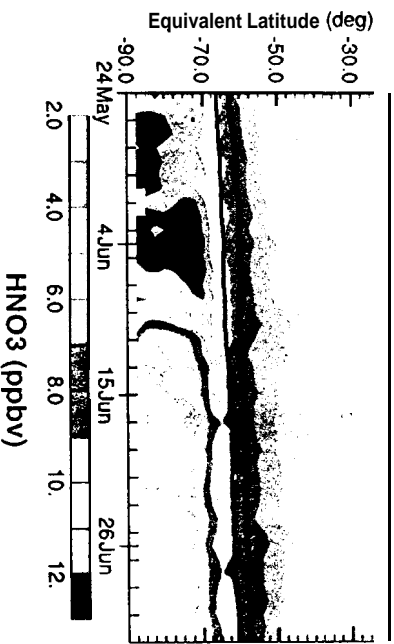
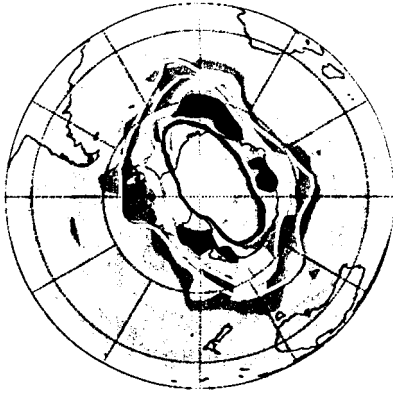


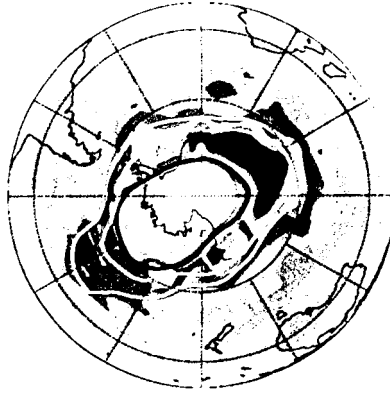
Plate 4

1994

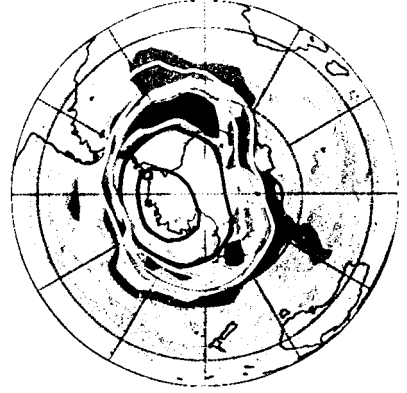
June 2



June 7



June 11



June 13



June 16



July 2

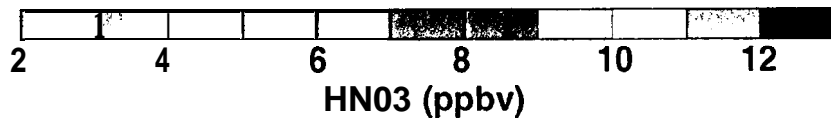
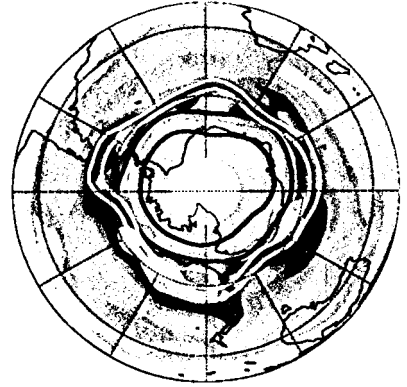
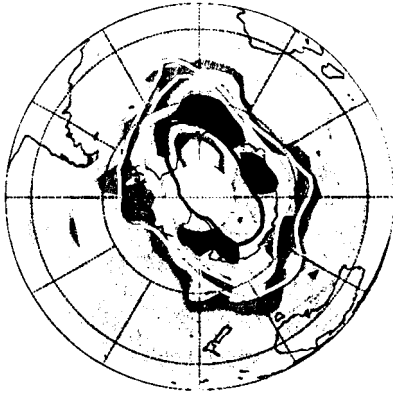


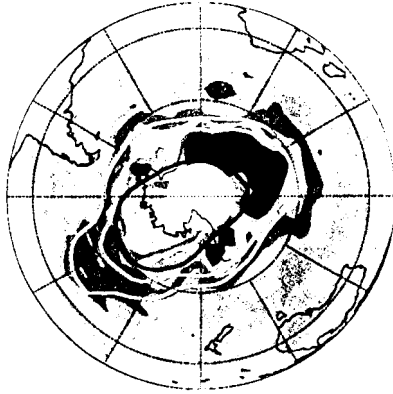
Plate 5a

1994

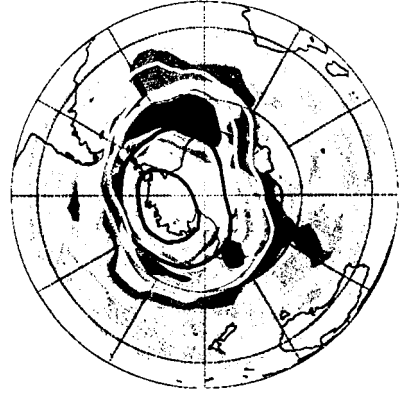
June 2



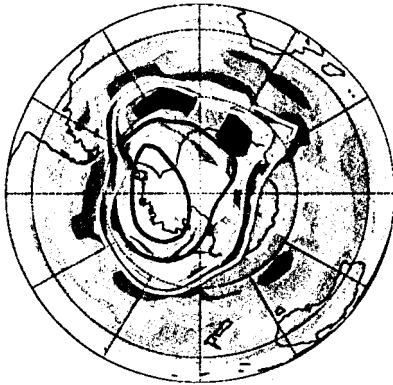
June 7



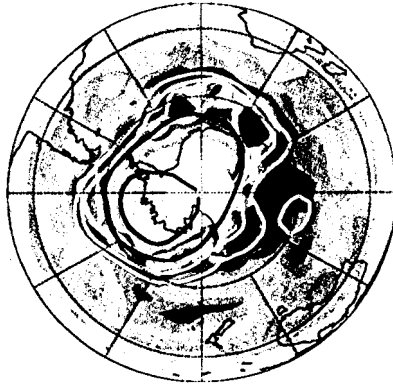
June 11



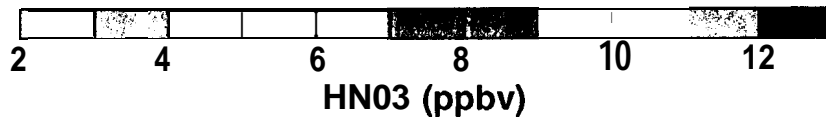
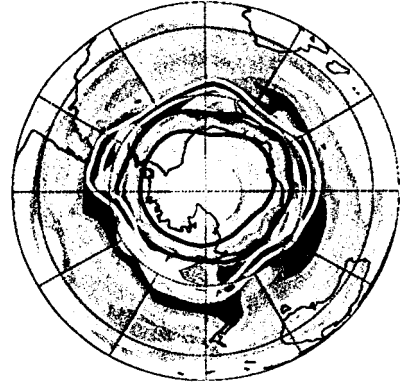
June 13



June 16

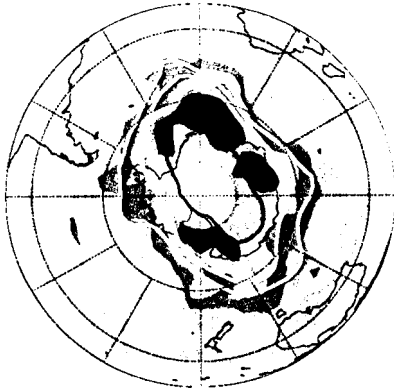


July 2

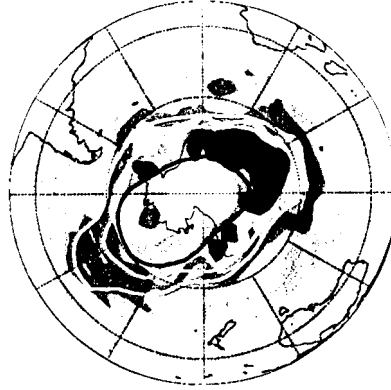


1994

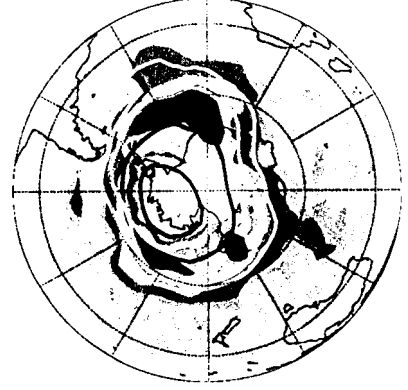
June 2



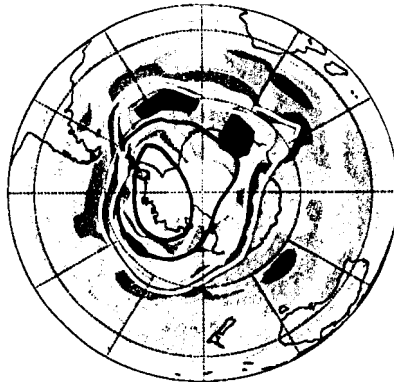
June 7



June 11



June 13



June 16



July 2

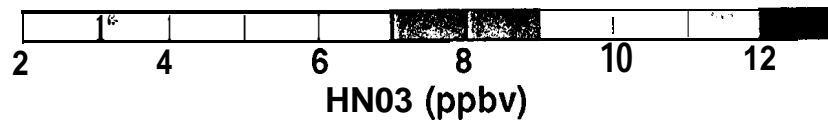
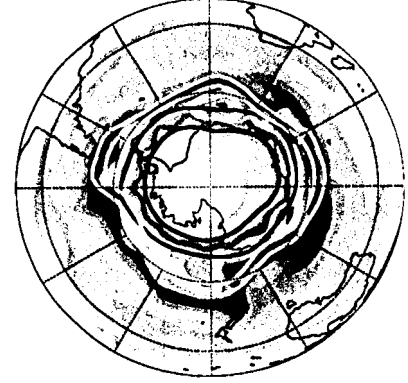


Plate 5c

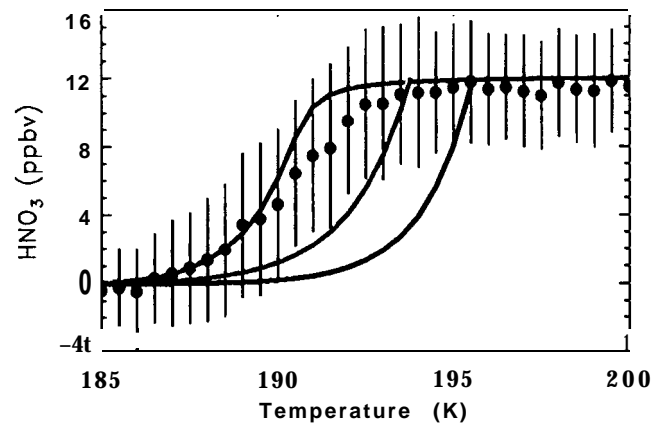
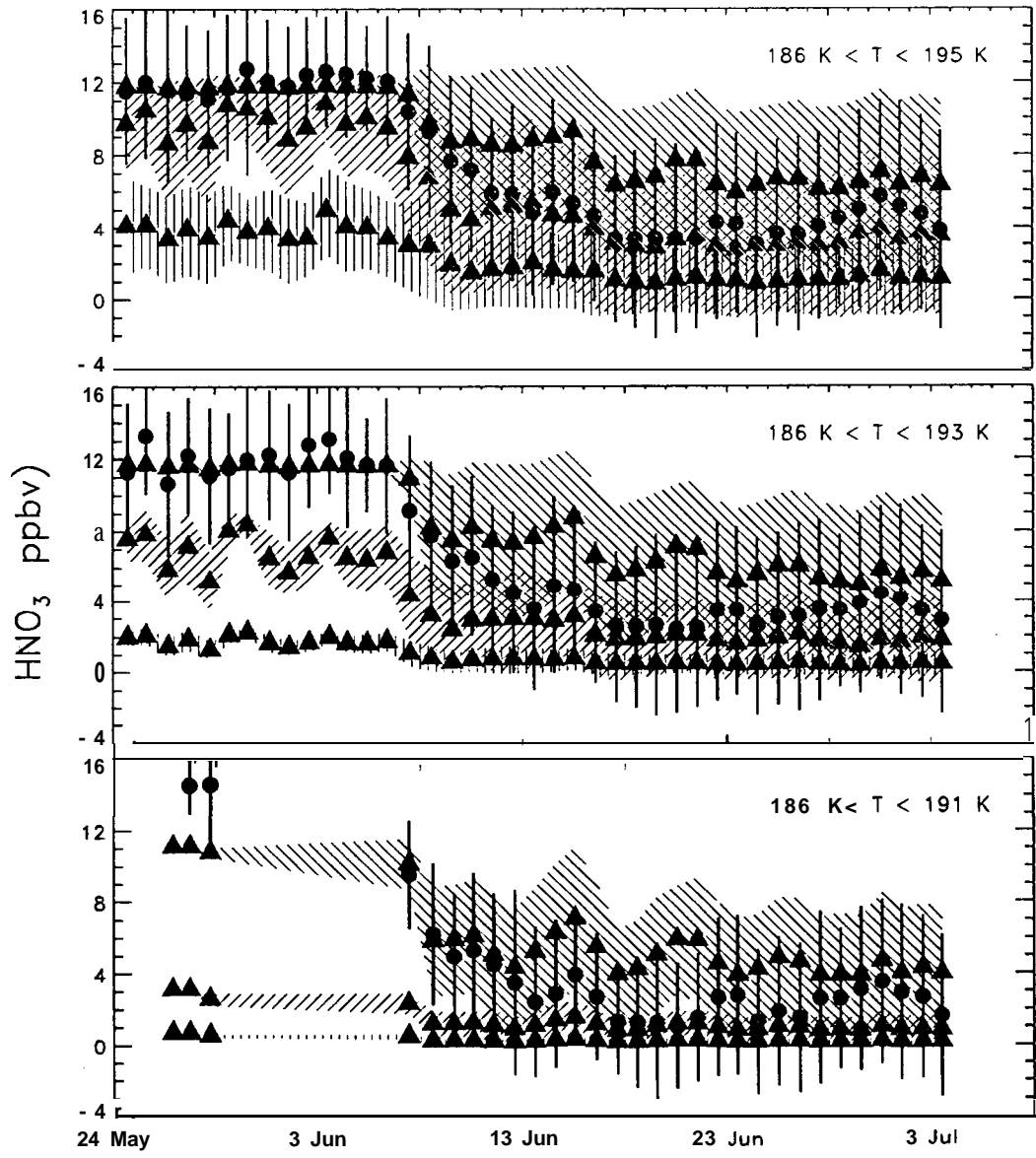


Plate 6



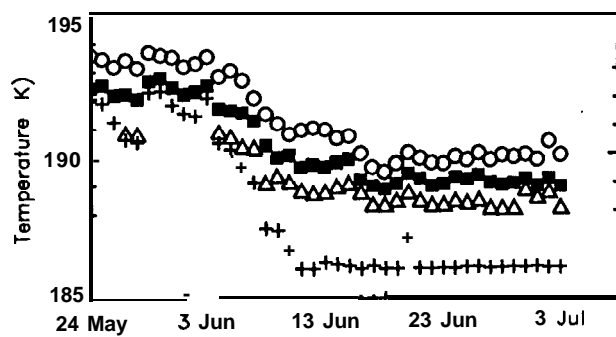
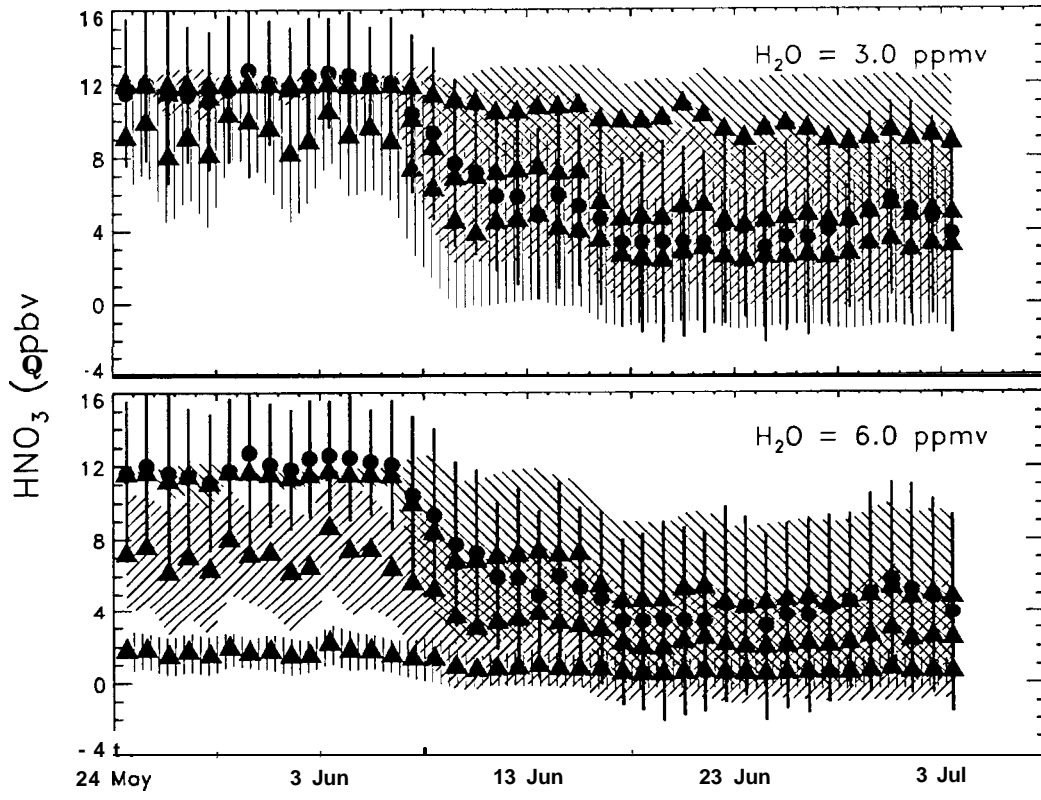
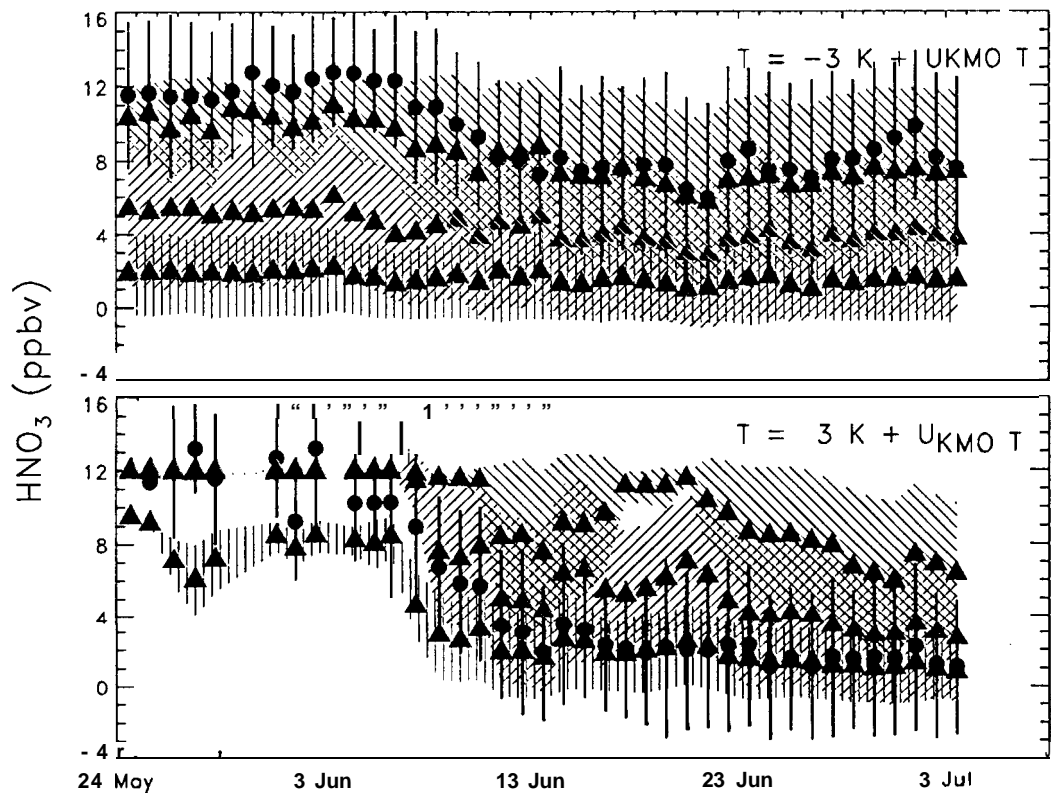
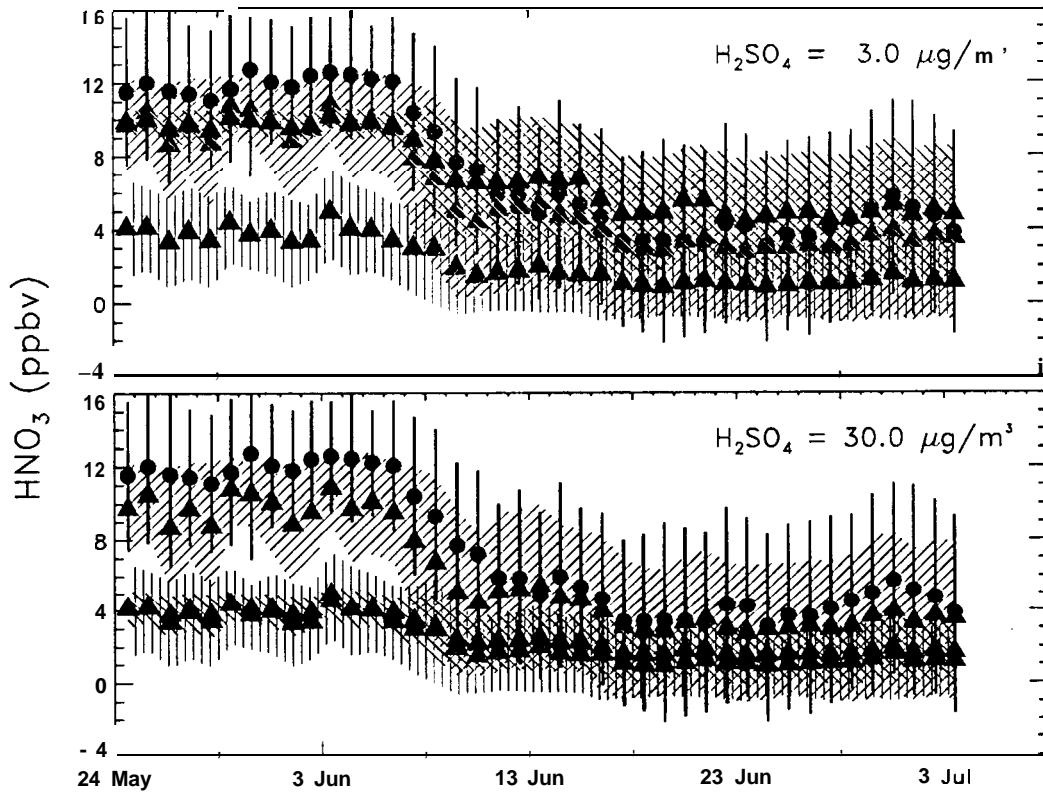
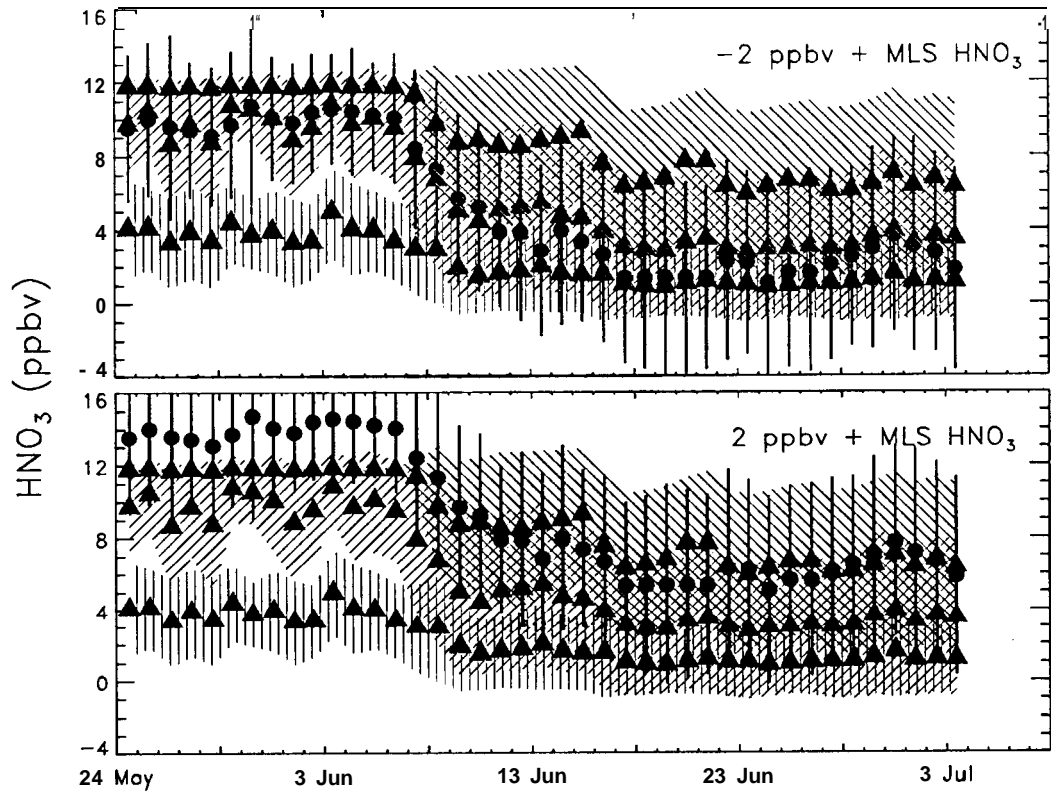


Figure 2





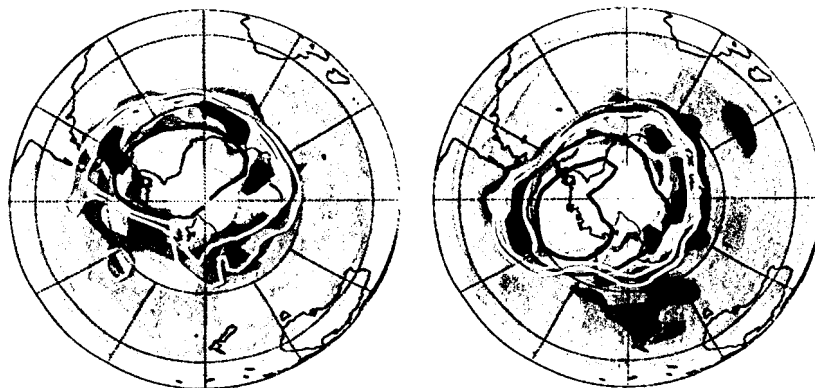




1992

June 2

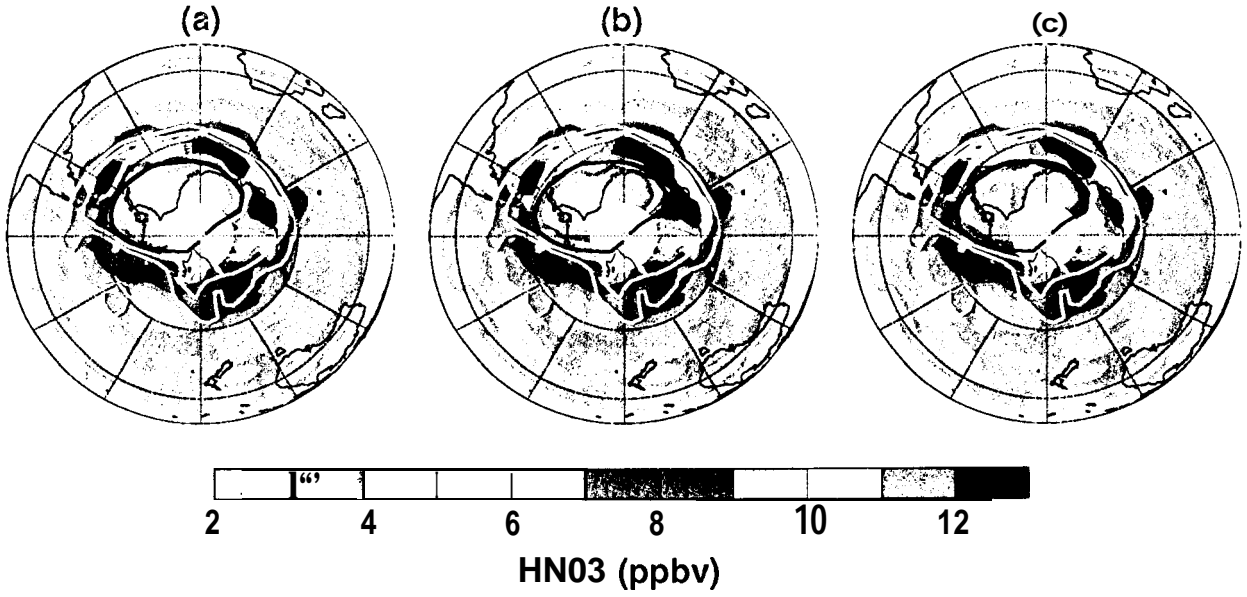
June 15



HN03 (ppbv)

Plate 9

1992



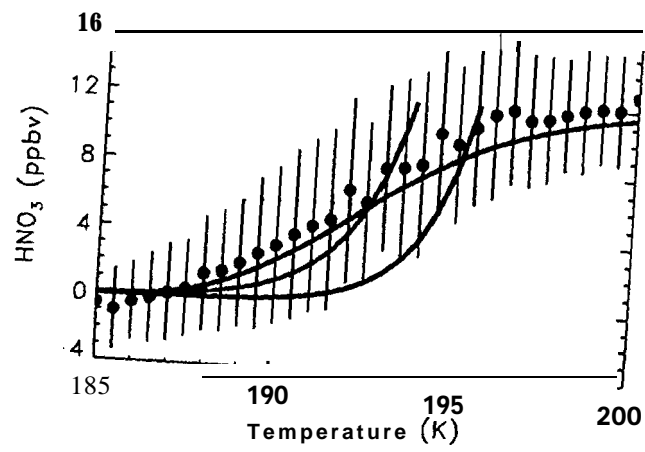


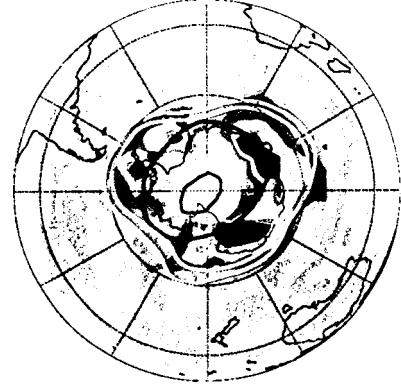
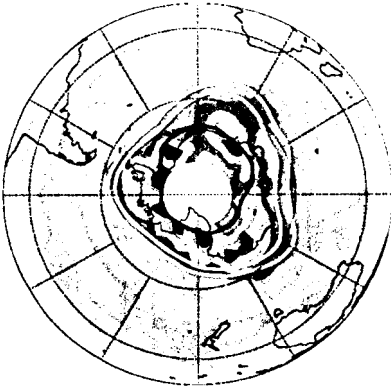
Plate II

1993

May 29

June 1

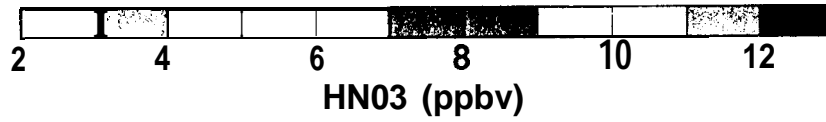
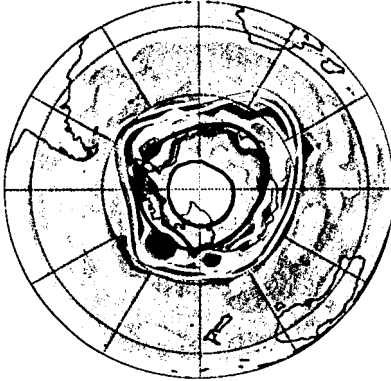
June 2

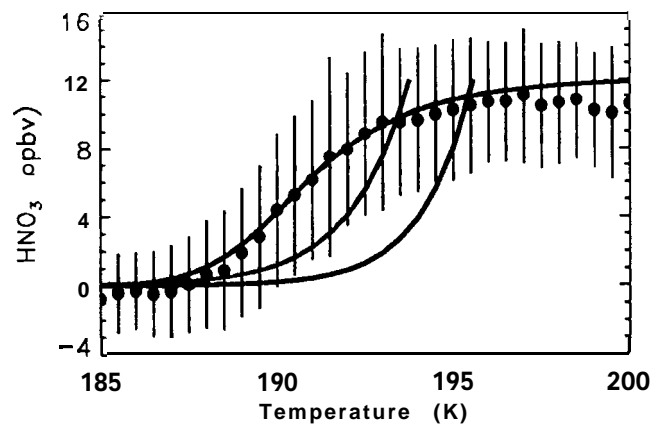


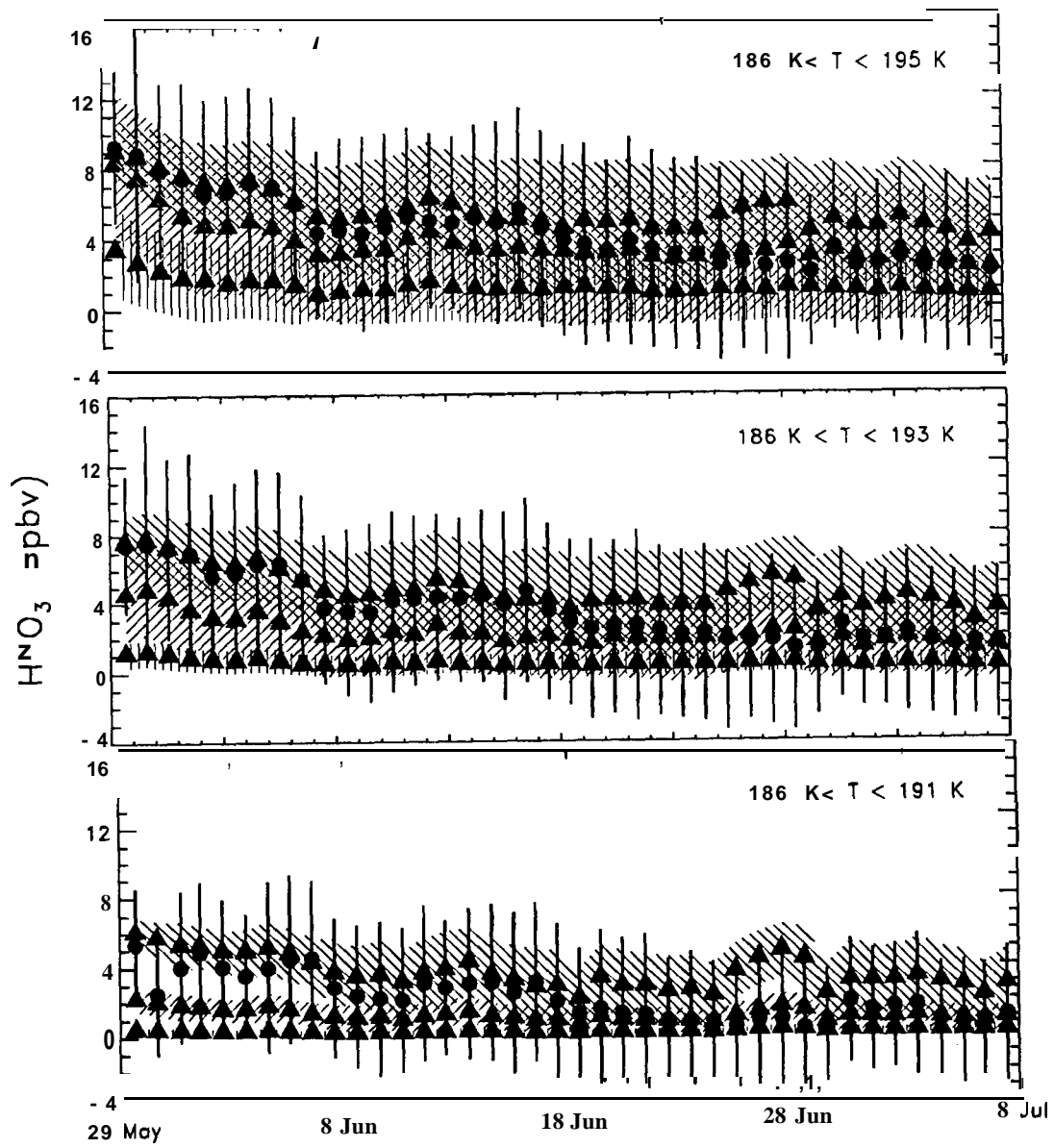
June 7

June 22

July 7



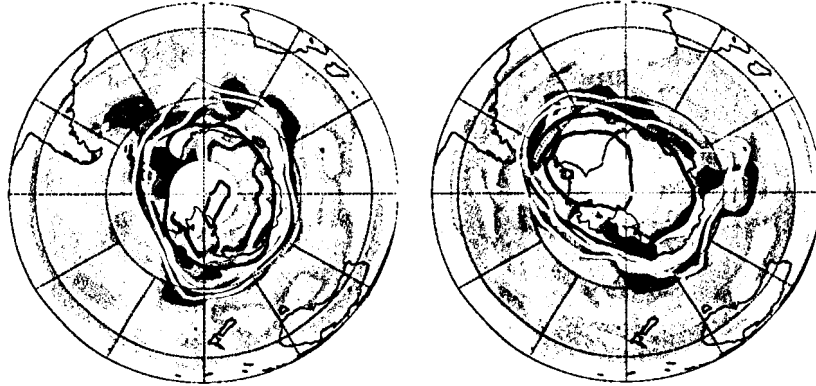




1995

June 7

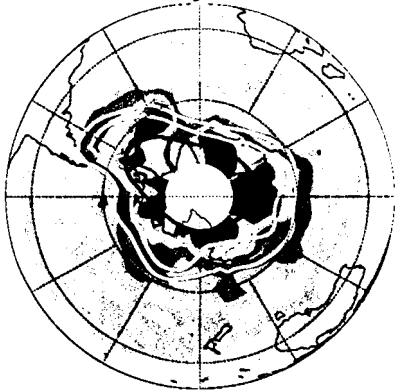
June 16



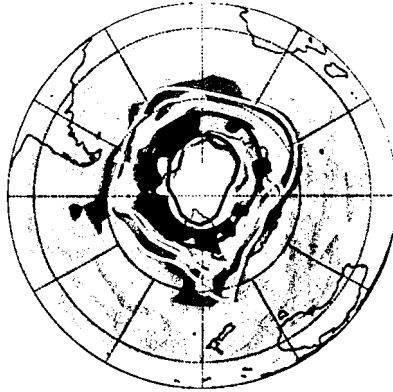
HN03 (ppbv)

1996

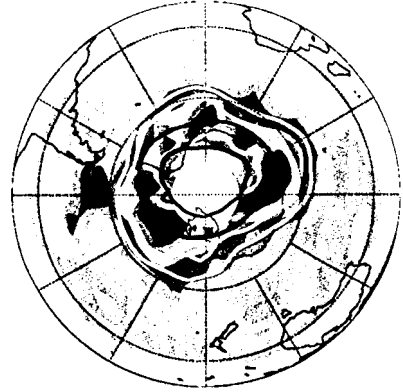
May 22



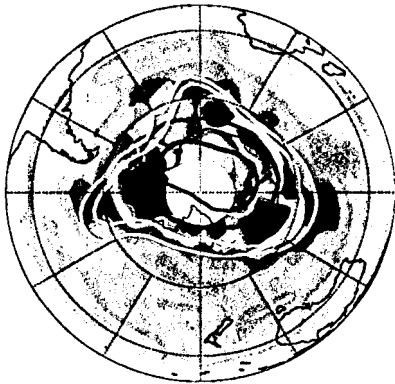
May 25



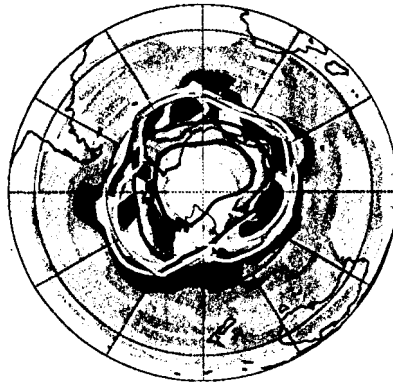
May 26



May 28



June 5



June 18

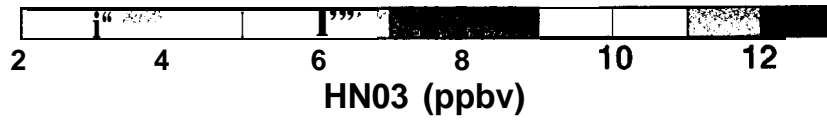
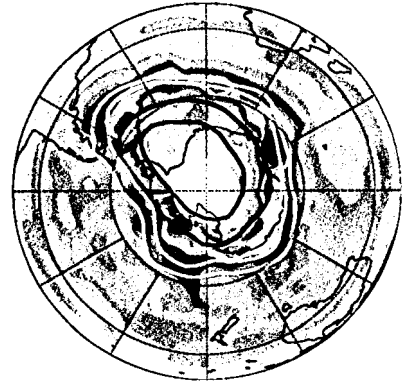


Plate 16

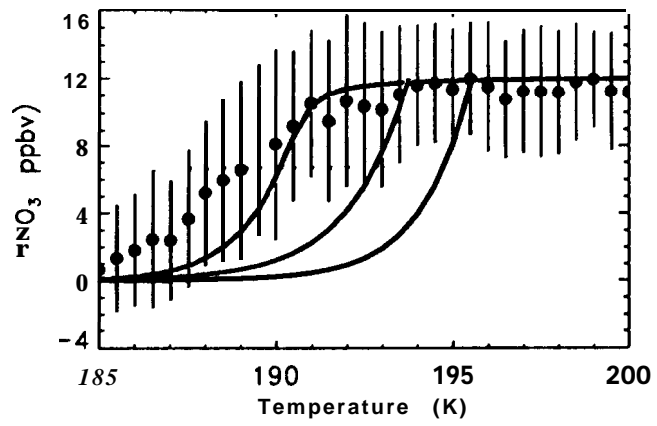


Plate 17

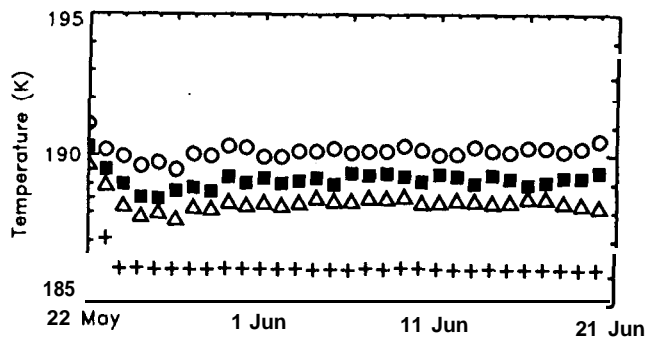
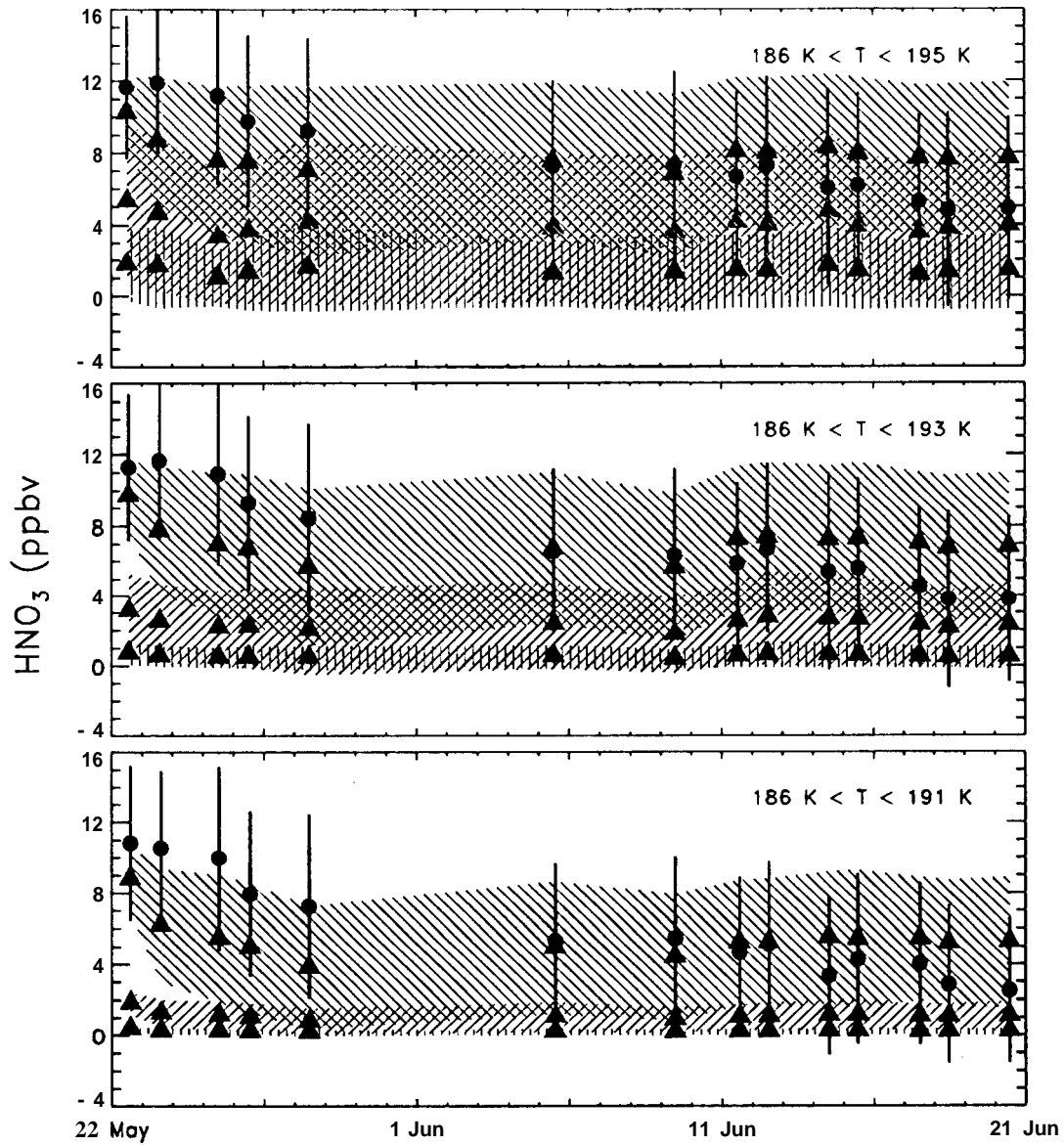
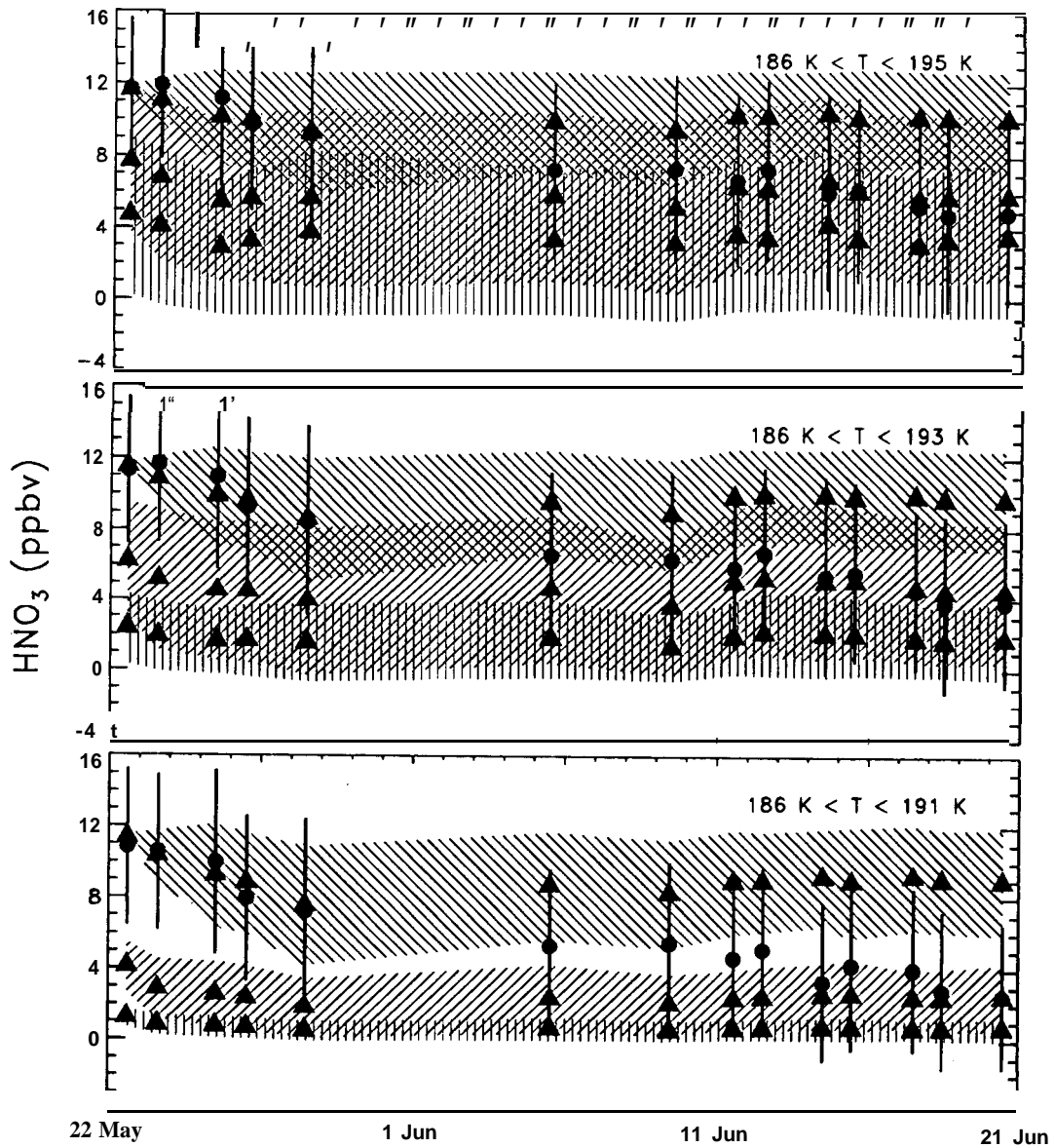


Figure 3





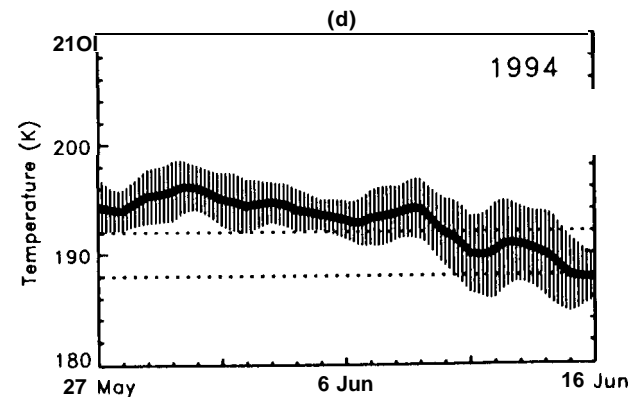
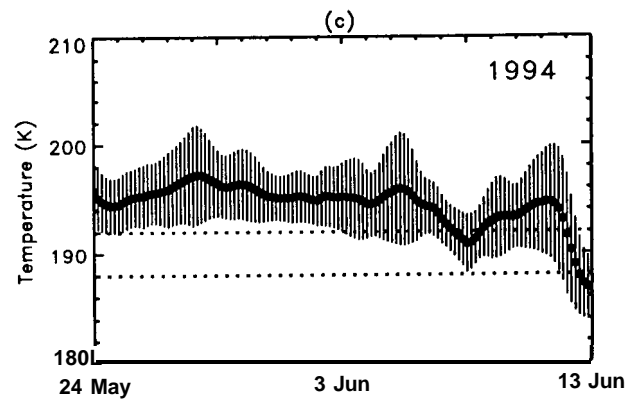
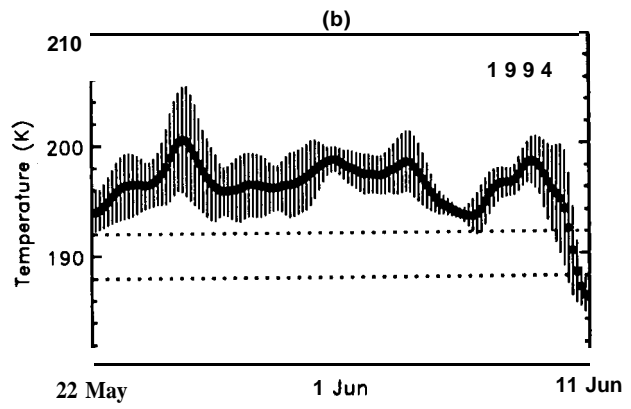
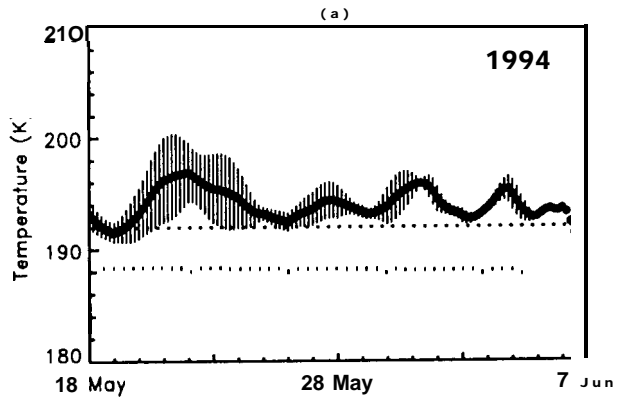


Figure 4

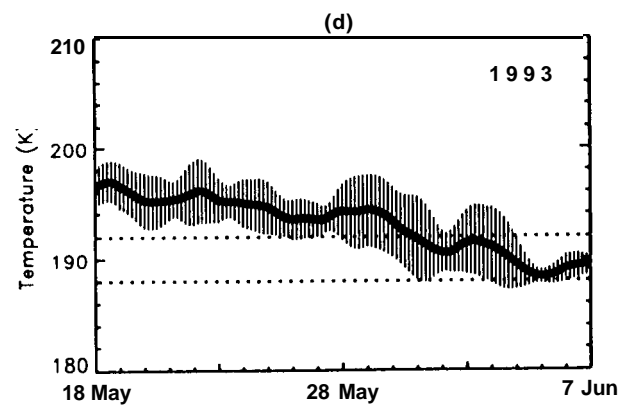
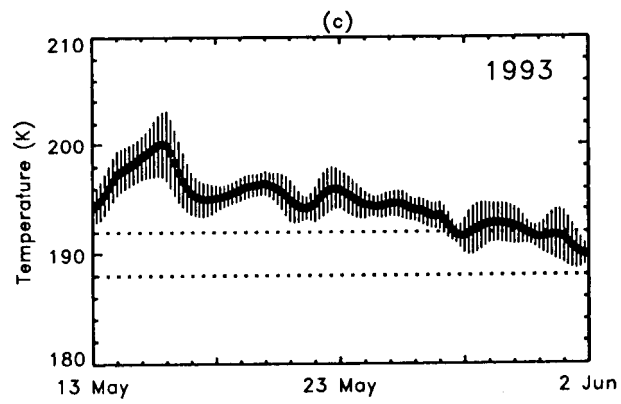
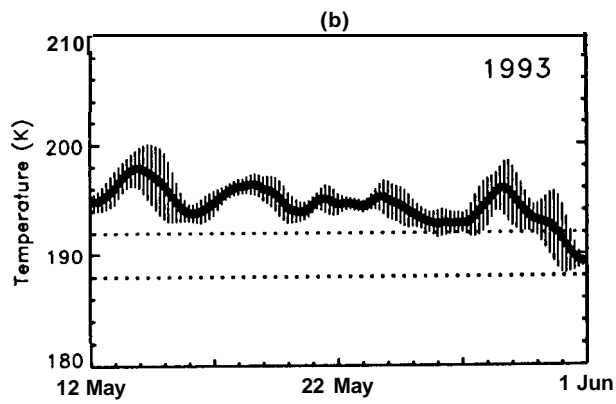
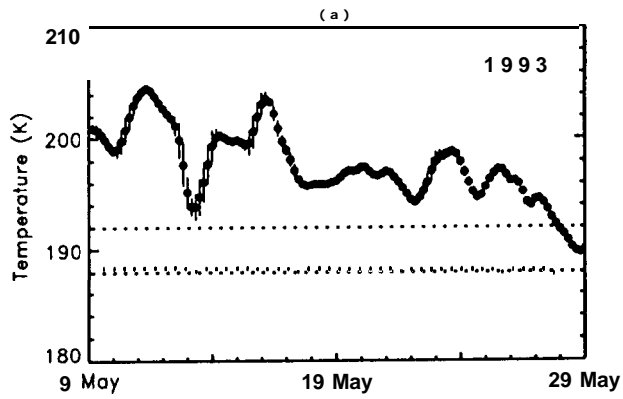


Figure 5

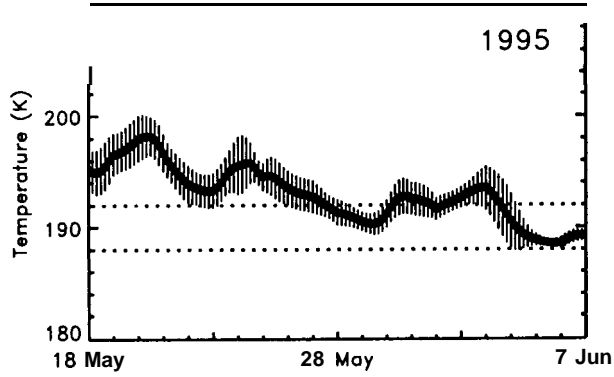
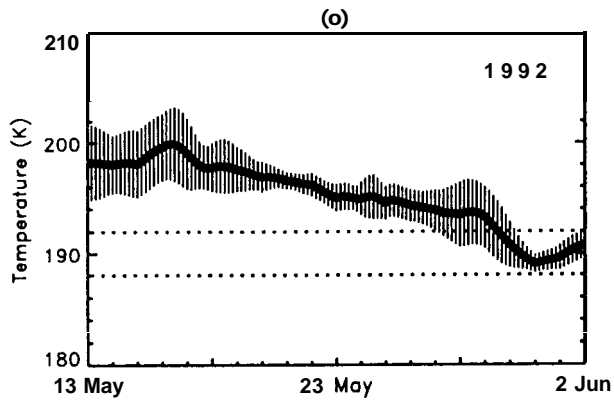


Figure 6

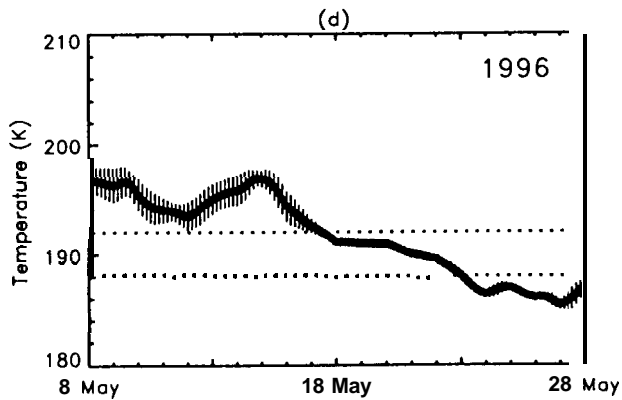
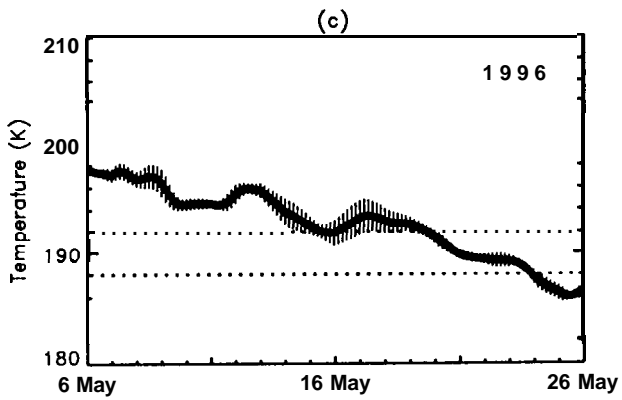
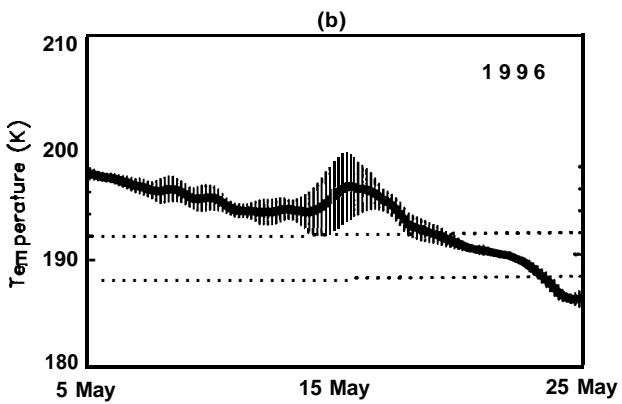
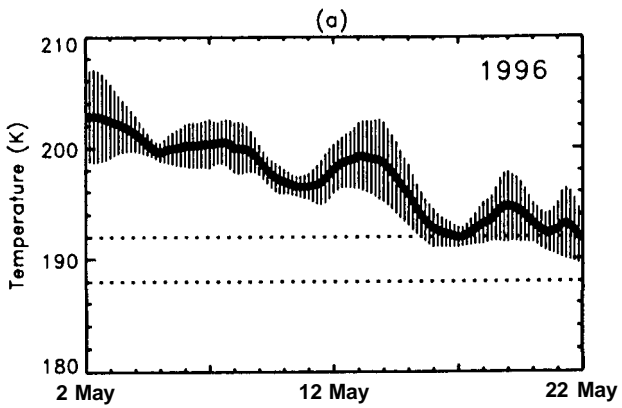


Figure 7